Palacký University Olomouc, Faculty of Science,
Department of Geoinformatics

Paris Lodron University Salzburg, Faculty of Natural Sciences,
Department of Geoinformatics

MONITORING THE EVOLUTION OF THE KAIWHATA LANDSLIDE IN NEW ZEALAND USING OBJECT-BASED IMAGE ANALYSIS AND SENTINEL-2 TIME SERIES

Diploma thesis

Author

Kiarash POOLADSAZ

Supervisor (Palacký University Olomouc)
RNDr. Jan BRUS, Ph.D.

Co-supervisor (Paris Lodron University Salzburg)
Mag. Dr. Daniel HÖLBLING

Erasmus Mundus Joint Master Degree Programme
Copernicus Master in Digital Earth
Specialization Track Geovisualization & Geocommunication
Olomouc, Czech Republic, 2023

ANOTATION

Landslides are geological events that occur frequently in mountainous and hilly areas of New Zealand, causing significant damage and changes to the landscape. These events can be disastrous, and monitoring their evolution and subsequent impacts is essential to mitigate hazards that could arise in later reactivation phases or similar cases. The abundance of time-series remote sensing data has facilitated the mapping and monitoring of landslides. Applying object-based image analysis (OBIA) allows for a more detailed understanding of the complex natural phenomena and help to integrate several type of features that are essential in the analysis and as the result, it facilitates to semi-automatically map the evolution of natural phenomena such as landslides. In this particular case, the focus is on the Kaiwhata landslide, which is located in the Wairarapa region of New Zealand. The data from Sentinel-2 and PlanetScope have been used from 2017 to 2021 to semi-automatically map the Kaiwhata landslide and monitor its evolution and impacts on the upstream area. To achieve this, the author has defined an OBIA workflow, consisting of rulesets that applied to the time-series data to extract the landslides and landslide-dammed lakes. The workflow has been defined using different multiresolution segmentation (MRS) values, classification parameters, and class refinements. The desired classes have been visualized not only in static two-dimensional (2D) maps but also in interactive three-dimensional (3D) models to influence the augmented visual impression and semantic augmentation of the time-series landslide and landslide-dammed lake results. The results of the OBIA mapping reveal the extent and the gradual increase in the area of the landslides, with two major changes occurring in June 2019 and November 2020. These changes were followed by the formation of temporary landslide-dammed upstream lakes along the Kaiwhata River, due to the intense rainfall. Overall, OBIA allows for a more detailed understanding of the landslides and their evolution and help to identify patterns and features that are not easily detectable by pixel-based approaches. The use of OBIA and time-series remote sensing data can provide valuable insights into the evolution of landslides and their impacts on the landscape.

KEYWORDS

DECLARATION

This thesis has been composed by *Kiarash Pooladsaz* for the Erasmus Mundus Joint Master's Degree Programme in Copernicus Master in Digital Earth for the academic years 2021/2022 and 2022/2023 at the Department of Geoinformatics, Faculty of Natural Sciences, Paris Lodron University Salzburg, and Department of Geoinformatics, Faculty of Science, Palacký University Olomouc.

Hereby, I declare that this piece of work is entirely my own, the references cited have been acknowledged and the thesis has not been previously submitted to the fulfilment of the higher degree.

22.05.2023, Olomouc   Kiarash Pooladsaz

ACKNOWLEDGEMENT

"Let yourself be silently drawn by the

strange pull of what you really love.

It will not lead you astray."

Rumi

Palacký University Olomouc
Faculty of Science
Academic year: 2022/2023

ASSIGNMENT OF DIPLOMA THESIS
(project, art work, art performance)

Name and surname: **Kiarash POOLADSAZ**

Personal number: **R210704**

Study programme: **N0532A330010 Geoinformatics and Cartography**

Work topic: **Monitoring the Evolution of the Kaiwhata Landslide in New Zealand using Object-based Image Analysis and Sentinel-2 Time Series**

Assigning department: **Department of Geoinformatics**

Theses guidelines

The main aim of the thesis is to verify the matter of multi-scale object-based analysis for increasing the accuracy of landslide mapping and monitoring. The student will identify the main spectral, spatial, and contextual parameters to apply for landslide and landslide-dammed lake classification for selected landslide and modify a single semi-automated object-based classification workflow for landslide time series analysis. The results will be temporal delimitations of landslides, maps, and interactive 3D web-based visualization application.

The student will attach all the collected datasets and all the animations to the thesis in digital form. The student will create a website about the thesis following the rules available on the department's website and a poster about the diploma thesis in A2 format. The student will submit the entire text (text, attachments, poster, outputs, input and output data) in digital form on a storage medium and the text of the thesis in two bound copies to the department's secretary.

Extent of work report: **max 50 pages**

Extent of graphics content: **as needed**

Form processing of diploma thesis: **printed**

Language of elaboration: **English**

Recommended resources:

Amatya, P., Kirschbaum, D., Stanley, T., & Tanyas, H. (2021). Landslide mapping using object-based image analysis and open-source tools. Engineering Geology, 282, 106000.

Ghorbanzadeh, O., Shahabi, H., Crivellari, A., Homayouni, S., Blaschke, T., & Ghamisi, P. (2022). Landslide detection using deep learning and object-based image analysis. Landslides, 19(4), 929-939.

Gudiyangada Nachappa, T., Kienberger, S., Meena, S. R., Hölbling, D., & Blaschke, T. (2020). Comparison and validation of per-pixel and object-based approaches for landslide susceptibility mapping. Geomatics, Natural Hazards and Risk, 11(1), 572-600.

Hölbling, D., Friedl, B., & Eisank, C. (2015). An object-based approach for semi-automated landslide change detection and attribution of changes to landslide classes in northern Taiwan. Earth Science Informatics, 8, 327-335.

Morgenstern, R., Massey, C., Rosser, B., & Archibald, G. (2021). Landslide dam hazards: assessing their formation, failure modes, longevity and downstream impacts. Understanding and Reducing Landslide Disaster Risk: Volume 5 Catastrophic Landslides and Frontiers of Landslide Science 5th, 117-123.

Liashenko, D., Belenok, V., Spitsa, R., Pavlyuk, D., & Boiko, O. (2020, November). Landslide GIS modelling with QGIS software. In XIV International Scientific Conference "Monitoring of Geological Processes and Ecological Condition of the Environment" (Vol. 2020, No. 1, pp. 1-5). EAGE Publications BV.
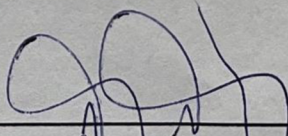
Supervisors of diploma thesis: **RNDr. Jan Brus, Ph.D.**
Department of Geoinformatics

Date of assignment of diploma thesis: **December 5, 2022**
Submission deadline of diploma thesis: **May 5, 2023**

L.S.

_____

doc. RNDr. Martin Kubala, Ph.D.
Dean

_____

prof. RNDr. Vít Voženílek, CSc.
Head of Department

Olomouc   December 5, 2022

CONTENT

LIST OF ABBREVIATIONS

Abbreviation	Meaning
2D	Two-Dimensional
3D	Three-Dimensional
a.s.l	Above Sea Level
API	Application Programming Interface
CSS	Cascading Style Sheets
DEM	Digital Elevation Model
EO	Earth Observation
GIS	Geographic Information System
GUI	Graphical User Interface
HR	High Resolution
JS	JavaScript
LiDAR	Light Detection and Ranging
LINZ	Land Information New Zealand
MRS	Multiresolution Segmentation
NDVI	Normalized Difference Vegetation Index
NDWI	Normalized Difference Water Index
NIR	Near-infrared
OBIA	Object-based Image Analysis
PSI	Persistent Scattered Interferometry
RF	Random Forest
RGB	Red Green Blue (colour model)
SAR	Synthetic Aperture Radar
SAVI	Soil Adjusted Vegetation Index
SVM	Support Vector Machine
UAV	Unmanned Aerial Vehicles
VHR	Very High Resolution
W3C	World Wide Web Consortium

INTRODUCTION

Landslides are a common hazard in many parts of the world and can result in significant damages on infrastructure and losses of life, landscape changes, reduction in agricultural activities, and huge economic losses. They can be triggered by natural factors such as intense rainfalls and earthquakes, as well as human activities such as deforestation and construction. They occur in different scales, from a major landslide to regional events with thousands of landslides. In addition, the landslide classification modified by Hungr et al. (2014) presents 32 landslide types, highlights the complexity of these natural phenomena. With climate change and population growth, the frequency of landslides and the number of people affected by them are increasing. New Zealand is one of the countries that is highly prone to landslides due to its geological features and location. Mountainous terrain with steep slopes, together with intense rainfall patterns and tectonic activities, result in highly susceptible areas to landslide failures in New Zealand. The main damages from landslides in this country include road closure, soil degradation, pasture productivity losses, river sedimentation, and loss of water quality (Rosser et al., 2017). The damages and complexity of the landslides trigger advanced image analysis methods for landslide mapping and monitoring the activation and evolution of landslides over time.

For several decades, visual interpretation of aerial imagery combined with field surveying have been considered as the common procedures in landslide mapping around the world, in which the expert manually delineates the landslide; however, this procedure is time-consuming, resource-intensive, and timely unavailable (Martha et al., 2010). In the recent years, Earth Observation (EO) data from different high resolution (HR), very high resolution (VHR) optical and synthetic aperture radar (SAR) sensors have facilitated the rise of new approaches to investigate the landslides. The availability and open-source feature of EO satellites programmes such as Copernicus Sentinel missions have paved the way to new emerging cost-effective methodologies. The European Union's Earth Observation Programme, Copernicus, which provides multispectral high-resolution data with 13 spectral bands and different spatial resolutions (up to 10 m for Red, Green, Blue (RGB) and Near-infrared (NIR) bands) with the repeat cycle of five days (Drusch et al., 2012). Sentinel-2 with 10 m resolution and high revisit time provides a rich resource of optical data for monitoring landslides. Despite the abundancy of EO data, providing a common methodology for recognising and monitoring landslide failures is yet challenging. Landslides lack distinguishable and identical spectral, spatial and temporal characteristics and the texture feature of the landslides can vary, influenced by geomorphological and hydrological factors besides weather conditions (Zhong et al., 2020). This diploma thesis aims to assess the efficiency of Object-based Image Analysis methodology to semi-automatically map the major landslide, the case study of Kaiwhata landslide, and monitor its evolution and the following risks that were accompanied by, using Sentinel-2 satellite images between 2017 and 2021. In addition, it is aimed to provide a 3D web model to improve the information transferability in a three-dimensional environment that helps to understand the evolution of the Kaiwhata landslide.

1 OBJECTIVES

This diploma thesis aims to explore the efficiency of OBIA methodology in time series landslide evolution monitoring. In addition, the suitability of Sentinel-2 satellite multi temporal images to monitor a major landslide will be evaluated. In addition, 3D web visualization application will be provided to foster the visualization of the results.

The methodological goals of the analysis part of this study are:

i. Verifying the matter of multi-scale object-based analysis for increasing the accuracy of landslide mapping,

ii. Identifying the main classification parameters to apply for landslide analysis,

iii. Modifying a single semi-automated object-based classification workflow for landslide time-series analysis,

iv. Providing an interactive 3D web visualization and storytelling for visualization that supports the better understanding of the phenomenon for different involved groups.

The visualization goal of this study is to provide 3D web visualization and storytelling visualization that help to comprehend the time-series landslide changes in the interactive and narrative approach. Providing the results in a 3D environment enables the potential involved people to realise the evolution of landslide in an interactive way through the time series of the results.

2 STATE OF ART

This chapter aims to cover the main topics regarding the role of EO data in developments in landslide detection and monitoring, recent approaches in landslide analysis, the applications of OBIA in landslide mapping and monitoring, and the 3D visualization technology advancements.

Landslide Hazards, Risks, and Disasters

Natural hazards can cause severe damage to infrastructure, human settlements, and land when a massive volume of mass-movement is involved (Alexander, 2005). Landslide failure is defined as the downward or outward displacement of debris, the mass of rock, residual soil, and sediments due to gravity (Cruden, 1991). It can be triggered by natural events such as volcanoes, earthquakes, and intense rainfall or human interventions, including road construction and land use changes (Hölbling et al., 2016). Global patterns of severe damages from landslides illustrate that landslides are a major hazard, particularly in areas with high rates of tectonic activities, high relief, and intense rainfall (Petley 2012). Morphologically, diverse types of erosion, such as fluvial, water, wave, and glacial, along a slope provides a complex condition that causes landslide failures. Cruden and Varnes (1996) developed the system of landslide typology and identified twenty-nine classes that are based on movement types and diverse types of materials, which shows the complexity of landslide types.
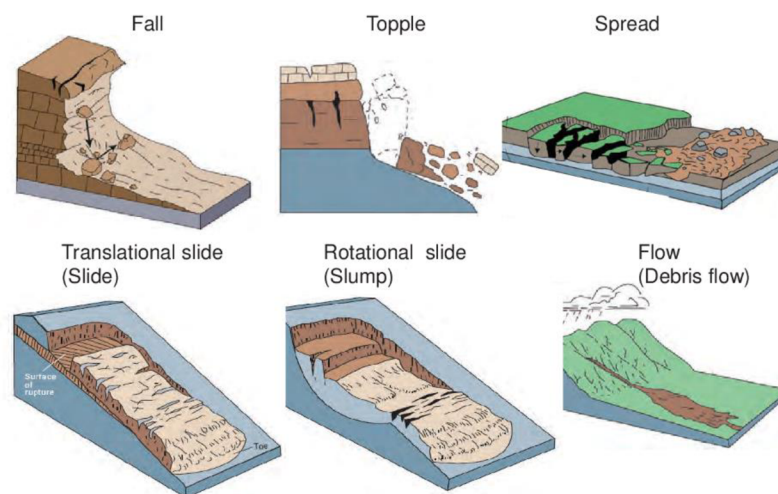
Figure 1. Landslide Movement Types (Cruden & Varnes, 1996)

New Zealand's geomorphological characteristics provide ideal conditions to host massive landslide failures, leading to damage costs of $250 to $300 million a year (Rosser et al., 2017). These damage costs stem from direct and indirect impacts on transportation, agriculture productivity, water quality and degradation of riverine habitat (Figure 2). The risk of landslides for the surrounding environment must not be ignored; not only the extent of damage that it leads to, but also the subsequent incidents that are followed by the failure exacerbate the degree of risks and damages (Dabiri et al. 2020). These incidents are not limited to but includes:

i. Landslide falling into a valley and block the river,
ii. The blockage forms a landslide dame that has the chance to fail when overtopped, causing a severe but short flooding,

iii.   Flooding the upstream before the dam fails,
iv.   The sediments can cause changes in river behaviour and slope, increasing sediment transport capacity, and flood risk (Davies, 2015).

Figure 2. Examples of landslides in New Zealand: a) Manutuke landslide triggered by cyclone Gabrielle, 2023; b) Whanganui landslide destroyed the state highway, 2019 (Images taken from Dave Petley's blog).

Earth Observation Data and Advancements in Landslide Analysis

Mapping landslide in the field is an old and common standard in landslide analysis. Field mapping usually comes with several difficulties such as where the size of the landslide is too big to be mapped, investigator viewpoint influences on recognizing different parts of the landslide, and distinguishing old landslide from the new one is challenging (Guzzetti et al., 2012). Visual interpretation of landslide with aerial photograph is another common approach to map landslides. A trained geomorphologist usually interprets the landslides using stereoscopic aerial photographs; however, it comes with uncertainties relying on human vision and manual mapping. In addition, this approach is usually resource-intensive, time-consuming, and timely unavailable (Martha et al., 2010).

EO data have enabled more efficiently monitoring of landslides and related hazard analysis compared to traditional measurements. Different sensors from space-, airborne, to ground-based platforms have become a crucial tool for landslide related studies, depending on the spatial coverage, available data for the desired duration time, and the purpose of the implementation (Lissak et al., 2020). Optical imagery including high-resolution (HR) and very high-resolution (VHR) satellite images, unmanned aerial vehicles (UAVs), synthetic aperture radar (SAR) data, and LiDAR data have become ubiquitous and cost-effective resources for many specific studies related to landslides recognition and inventory mapping, change detection, susceptibility mapping, landslide volume estimation, and so on at different scales (Mondini et al., 2021; Guzzetti et al., 2012; Xun et al., 2022; Hölbling et al., 2017; Karantanellis et al., 2020; Pawłuszek et al., 2019).

The abundancy of (free) timely satellite images highlights the value of space borne platforms that have become a reliant source for better understanding of landslide failures, including their distribution, size, and types and facilitates time-series analysis of the subsequent changes, such as dams, lakes, and post-disaster damage assessment (Hölbling, 2022). Several studies aimed to monitor the evolution of the landslide over the prolonged period; however, they applied ground-based methods to acquire the data (Uhlemann et al., 2016; Travelletti et al., 2012). Using different satellite images such as Synthetic aperture radar (SAR) and optical imagery, researches have focused on change detection using pre- and post-event images to map the landslide failures (Mora et al., 2018; Lu et al., 2019; Plank et al., 2016; Hölbling et al., 2015). Utilizing time-series

satellite images to study the gradual changes of landslides enables assessing the landslide activity, its evolution, and their following impacts on their environment. This approach is followed by researches such as in Tofani et al. (2013), where they used SAR images and Persistent Scattered Interferometry (PSI) approach together with ground-based data for characterizing and monitoring the landslide displacement mechanism. Behling et al. (2014) suggested time-series analysis to identify landslides and their changes based on NDVI trajectories using optical satellite images. Yang et al. (2019) used Sentinel-2 time series to analyse Normalized Difference Vegetation Index (NDVI) indices to detect slope movement before the landslide failure occurs. Abad et al. (2022) addressed the spatiotemporal evolution of landslide-dammed lakes using Sentinel-2 imagery for disaster mitigation.

Object-Based Image Analysis (OBIA)

Pixel-based image analysis methods have been traditionally applied to landslide detection and mapping (Pawluszek et al., 2018; Mondini et al., 2017). This method focuses mainly on spectral information of single pixels. Several researches have highlighted that pixel-based image analysis is prone to false detection and therefore, salt-and-pepper effect when analysing complex phenomena like landslides (Hölbling et al., 2012; Blaschke et al., 2014; Heleno et al., 2016). OBIA method has gained attentions due to its more satisfying results in landslide mapping, where the method interlinks spectral, spatial, contextual and morphological information in multiple scales (Lang & Blaschke, 2006).

The availability of high-resolution images has generated multiple challenges for per-pixel analysis considering objects, shape, texture, context and pattern, semantics, and knowledge integration (Blaschke et al., 2014). The natural and built-up environment consists of several types of substances, but also spatial features related to an object or neighborhood relationships and topological properties (Lang & Blaschke, 2006). Having a shift from per-pixel analysis where spatial patterns where left out of the classic image analysis approach, as Figure (3) shows, Segmentation constructs the initial bridge from pixels to OBIA, providing the possibility to delineate boundaries based on homogeneity in spectral and continuous values and therefore, the building blocks of OBIA would be provided (Blaschke et al., 2014). Spatial features add meaningful layers towards classification in OBIA, where it helps reduce the salt-and-pepper effect (Blaschke & Strobl 2001) and assigning the image segments into more meaningful classes.
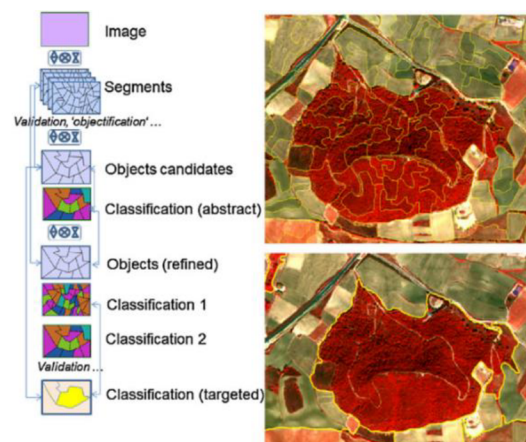

Figure 3. Segmentation as the initial bridge from pixel to OBIA workflow (Blaschke et al., 2014).

As mentioned by Lang & Tiede (2015), spatial features define the objects at an individual level, for example water may be considered as a lake or a river, also in different levels (scales), where nested hierarchy of a class in the super-object is related to multiple classes into sub-objects (Figure 4). In addition, the hierarchy principle follows the ideas behind human image perception. Human vision receives signals from the environment and the signals are processed to form structural attributes in different levels of perception. Several ideologies such as Gestalt principles attempted to simplify the complexity of image perception (Ward et al., 2014). Gestalt principles reflect the fact that image perception stems from set of interaction in the continuous space, reification or in another term, objectification of a complex set of relationships.
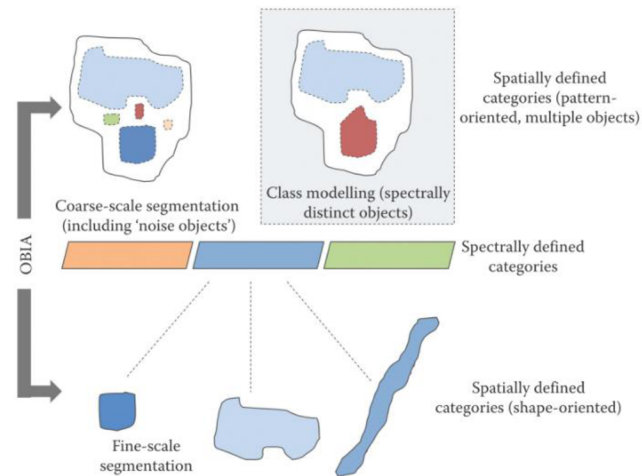
Figure 4. Influence of spatial attributes on spectral categories in OBIA (Lang & Tiede, 2015)

Decomposing the complex scene needs knowledge-based rules to be applied comprising spatial features that helps evaluating the horizontal relationships among objects and providing the possibility to extract the class(es) of interest into the semantic approach, as called class modelling (Tiede et al. 2010). In addition, the decomposition focuses on providing a set of sub-objects in the vertical way that would help the comprehension of the whole scene in a hierarchical view and make the output more efficient (Figure 5).
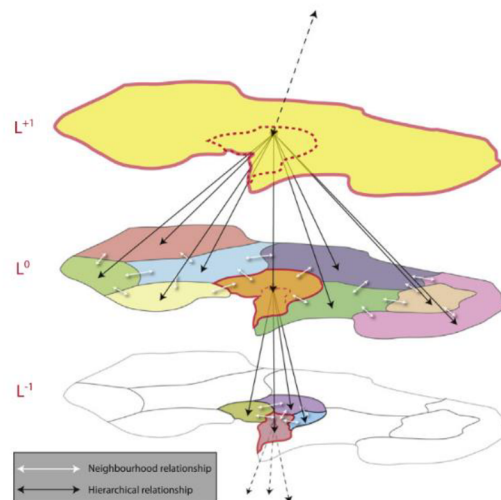
Figure 5. Hierarchical relationship (such as "is-part-of" or "consists-of") beside neighborhood relationship (Blaschke et al., 2014)

For this standpoint, multi-scale segmentation offers different levels of object decomposition, from homogenous objects based on spectral value aggregation, as called level of elementary landscape units (Lang & Blaschke, 2006), to higher levels where the internal heterogeneity is increasing but there would be more concentration on functional homogeneity.

OBIA makes bridges between remote sensing, GIS and image processing, considers segments as the initial block of the analysis associated with explicit knowledge to reach customized classification. Proposing the spatial, morphological, contextual, and hierarchical contexts to spectral properties could help comprehending and interpreting the images with semi-automatic ways (Hay & Castilla, 2008) and complement the spectral properties to reach more semantic content.

Landslide Analysis and Monitoring with OBIA Methodology

Developments in remote sensing and OBIA semi-automated and automated methods have improved the ability to map landslides with less human interaction (Amatya et al., 2021). As mentioned before, OBIA demonstrates advances over pixel-based approaches when mapping complex natural features such as landslides, which consist of twisted textures and extreme spectral heterogeneity, considering the extent, types, and distribution of the failure (Hölbling et al., 2015). Landslide features are not limited to spectral signature, but also topographic, morphological, and contextual features must be considered (Martha et al., 2010). The advances in landslide analysis and mapping in OBIA stem from the multi-scale integration of spectral information (colour), spatial properties (e.g., size, shape), textural data (e.g., surface disturbance difference), and contextual information (e.g., relationship with neighbouring objects) (Blaschke et al., 2014). This integration combined with other datasets, such as a Digital Elevation Model (DEM) and its derivatives, have provided promising results (Hölbling et al.,2017, 2020; Martha et al., 2016; Blaschke et al., 2014; Amatya et al., 2021; Karantanellis et al., 2020).

Semi-automated OBIA approaches for landslide analysis have been employed in studies that combine image analysis and machine learning methods with degree of expert knowledge. Stumpf & Kerle (2011) tested random forest (RF) machine learning technique on VHR optical images to minimalize the manual threshold and feature selection in landslide mapping. Amatya et al. (2021) provided a semi-automated landslide detection based on different open-source Python packages and modules. Pawłuszek et al. (2019) used LiDAR-derived terrain features with support vector machine (SVM) classification approach to evaluate its applicability for landslide identification through OBIA. Feizizadeh et al. (2017) applied fuzzy classification scheme within knowledge-based classification to detect landslides and their changes. Limited studies focused on time-series analysis in OBIA for landslide monitoring. Table (1) provides information about several researches that based on knowledge-based classification rules applied OBIA methodology to semi-automatically map and monitor landslide. The information regarding segmentation type and classification parameters will be beneficial when modifying the workflow of this diploma thesis. Meanwhile, as we discussed earlier, the parameters to map the landslides differ significantly due to the diverse characteristics and complexity of the failures.

Table 1. Related studies that focused on semi-automatic landslide mapping and monitoring based on knowledge-based classification rules.

Research Authors	Main Objective	Main Data	Desired Class	Segmentation Type	Classification Parameter
(Hölbling et al., 2020)	Semi-automatically mpping the evolution of landslide and discovering the correlation with heavy rainfall.	Optical images, DEM	Landslide	Multiresolution segmentation	NDVI, SAVI, Brightness, Slope, DEM
			Landslide-dammed		NDVI, near-infrared band
(Dabiri et al., 2020)	Mapping geomorphological features ,changes, and volume estimation from the landslide failure.	Optical and Radar images, ArcticDEM	Landslide	Multiresolution segmentation	Sentinel-1 VV intensity change layer, NDVI, slope, edge-extraction layer igma, object length
			Landslide-dammed		NDVI, Sentinel-1 VV intensity change layer
			Riverbed with water		edge-extraction layer sigma, NDVI, Object length
(Lahousse et al., 2011)	Semi-automatically mapping shallow landslides with a multi-scale approach	Optical image , DTM	Landslide	Multiresolution segmentation	NDVI, Brightness, Compactness, Length to width, GLCM mean of the red band, sub-objects stdev. Of mean NDVI, Relief to length, Relief to width
(Hölbling et al., 2017)	Detecting and delineating landslides in different cases to compare semi-automatica and manual mapping	Optical images, DEMs	Landslide case 1	Multiresolution segmentation	diff. To neighbors (NDVI), slope, Length/width
			Landslide case 2	Multiresolution segmentation	NDVI, Mean slope, brightness
			Landslide case 3	Threshold segmentation	Slope, TRI, size, Perimeter/ area ration, NDVI
			Landslide case 4	Threshold segmentation, Multiresolution segmentation	Same as 3 except: no NDVI
			Landslide case 5	Multiresolution segmentation	NDVI, slope, legnth/width, Shape index
(Martha et al., 2010)	Detecting and classifying landslides using combination of spectral, shape, and contextual infrormation	Optical image, DEM	Landslide	Multiresolution segmentation, Chessboard segmentation	NDVI, hillshade, near-infrared band, Brightness, slope, relief, length/width, GLCM homogeneity of the red band

Advancements in 3D Visualization Technologies

Advanced remote sensing technologies such as LiDAR (Light Detection and Ranging) and SAR (Synthetic Aperture Radar) and improved data processing algorithms have enabled obtaining detailed topography and elevation data with higher spatial resolution. Combining the Digital Elevation Models (DEMs) with high quality raster graphics provides pseudo three-dimensional (3D) representations (also known as 2.5D) and a top-notch navigation experience over the textured surface model of the real world that increase the user interaction and understanding (Evangelidis et al., 2018). 3D representations significantly allow for a more intuitive representation of the scene, bridge the gap between user and the expert through the interactive model, and improve the communication and informed decision-making processes (Juřík et al., 2020). In addition, the 3D surface impacts on an augmented visual impression and semantic augmentation that together help to support the concept of storytelling (Thöny et al., 2018). Many applications related to natural hazard monitoring (Preppernau & Jenny, 2015; Fiorucci et al., 2019), cultural heritage reconstruction (Dhonju et al., 2018), urban planning (Vitalis et al., 2020), ground water monitoring (Hunter et al., 2016), and cartography (Sieber et al., 2019) have utilized 3D visualization methods, thanks to computer graphic technologies, to provide an end-user interactivity through web browser.

The developments in 3D modelling visualization are supported by frameworks like WebGL JS API[1] to render the model by any web browser compatible with World Wide Web Consortium (W3C) open standards. WebGL JS API allows for real-time rendering of 3D objects and scenes that user can interact with the visualization in real-time with high performance and customize the function and usability. There are several examples of WebGL-based 3D geospatial visualization frameworks, such as:

- Three.js[2]: A JavaScript library for creating 3D graphics and animations in web browsers. While it is not specifically designed for geospatial visualization, it can be used to create 3D visualizations of geospatial data.
- CesiumJS[3]: An open-source JavaScript library that enables high-performance 3D geospatial visualization in web browsers. It provides a wide range of features, including support for 3D models, terrain, and imagery.
- Qgis2threejs[4]: A plugin for the QGIS software that allows users to create interactive 3D visualizations of geospatial data using the Three.js library and allows users to export their 3D visualizations as HTML files, which can be easily embedded in websites or shared with others.
- Deck.gl[5]: a WebGL-powered framework for building advanced data visualization applications, including spatial 3D visualizations. Developed by Uber, it supports a range of 3D geospatial data types, including point clouds, meshes, and terrain data.

These frameworks are just a few examples of the WebGL-based frameworks available for creating 3D geospatial visualizations. Each follows its set of features and capabilities, and therefore, it is important to determine the best fit for a particular case.

---

[1] https://www.khronos.org/webgl/
[2] https://threejs.org/
[3] https://cesium.com/platform/cesiumjs/
[4] https://plugins.qgis.org/plugins/Qgis2threejs/
[5] https://deck.gl/

3 METHODOLOGY

This chapter introduces the study area of this diploma thesis, the different data that have been utilized, and the software that have processed the analysis. In addition, the workflow of this diploma thesis is provided to highlight the data acquisition, analysis, and final visualization of the results.

3.1 Study Area

The study area is located in the south of New Zealand's North Island, within the Wairarapa geographical region, east of Wellington (Figure 6). The area covers 9.7 km² and is characterised by the Kaiwhata River, which flows to the southeast reaching the Pacific Ocean. The topography of the study selected area varies from 10 m to 500 m a.s.l. and is mainly covered by grassland and forest areas accessed through the Kaiwhata road.
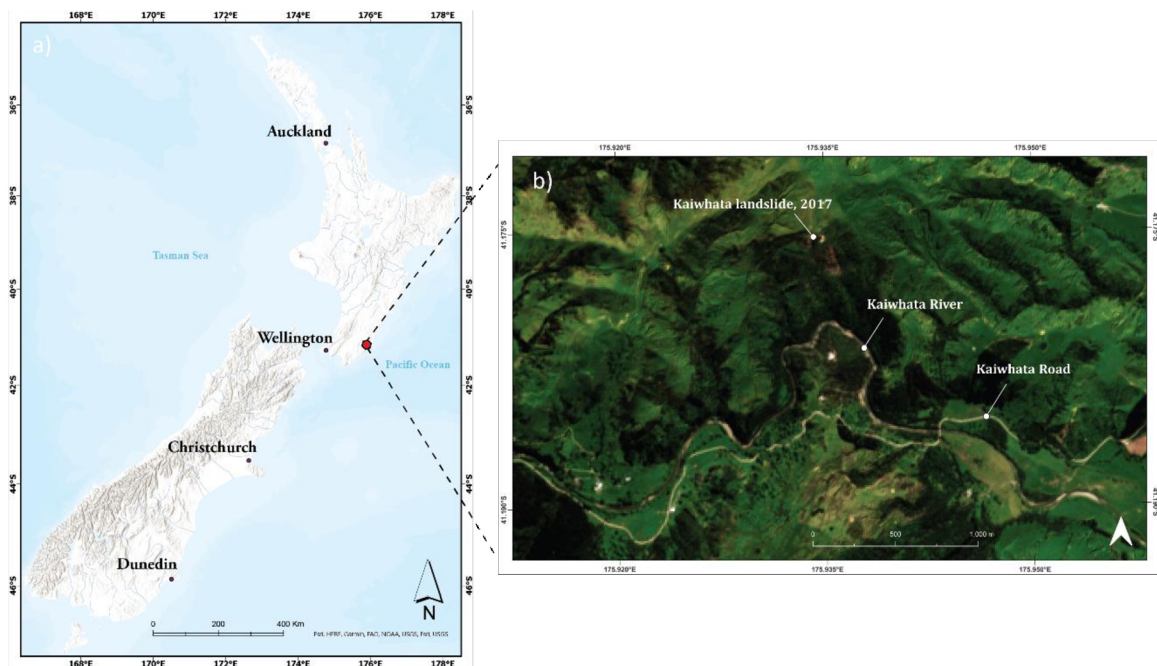

Figure 6. a) Location of the study area in the south of North Island, New Zealand (background data: © ESRI); and b) Study area shown by Sentinel-2 satellite image from 13 October 2017.

The initial landslide failure that occurred in 2017 was comparatively small. The second landslide failure on 1 June 2019 near the Kaiwhata River (Figure 7) was significantly larger. The debris set up a landslide dam, which lasted approximately two weeks, formed an extensive upstream lake, and closed the Kaiwhata road. Due to the uprising level of the lake (overtopping), the formation of a minor water channel towards downstream, and the material specifications, the dam failed and released around 1.1 M m³ of water in less than two hours to the downstream area (Morgenstern et al. 2021).
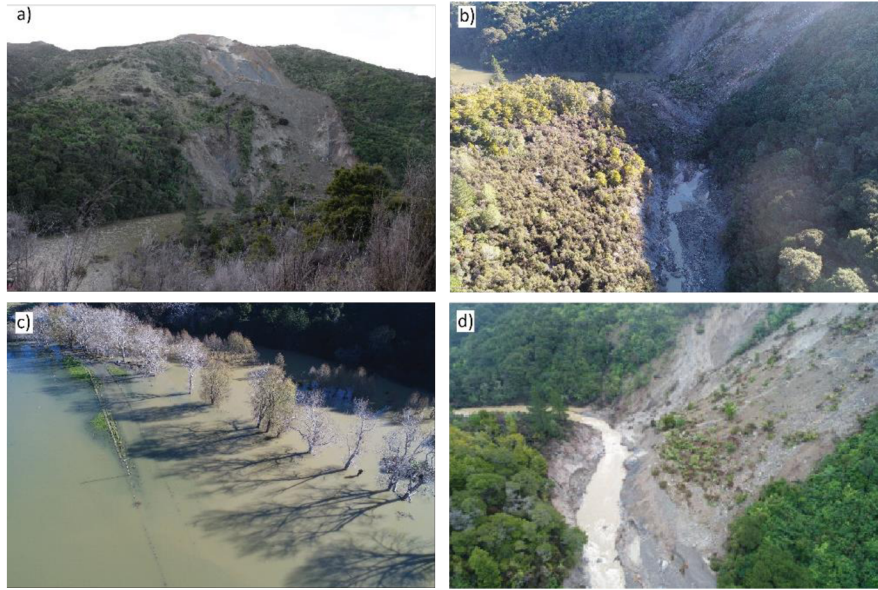
Figure 7. a) South-to-north view of the second landslide failure (photograph: © B. Rosser; 6 June 2019); b) Landslide formed a dam and blocked the river (photograph: © R. Morgenstern; 6 June 2019); c) Lake was formed upstream and flooded the land and infrastructure (photograph: © R. Morgenstern); d) Dam failed and enormous amount of water went downstream (photograph: © R. Morgenstern; 14 June 2019).

This cycle of incidents occurred again from November 2020 to January 2021 (Figure 8). The landslide was reactivated after heavy rainfall in November 2020 and damaged adjacent properties, lands, the main road, and infrastructure (Anselm, 2020). Subsequently, the landslide-dammed lake overtopped the dam, and the dam failed.

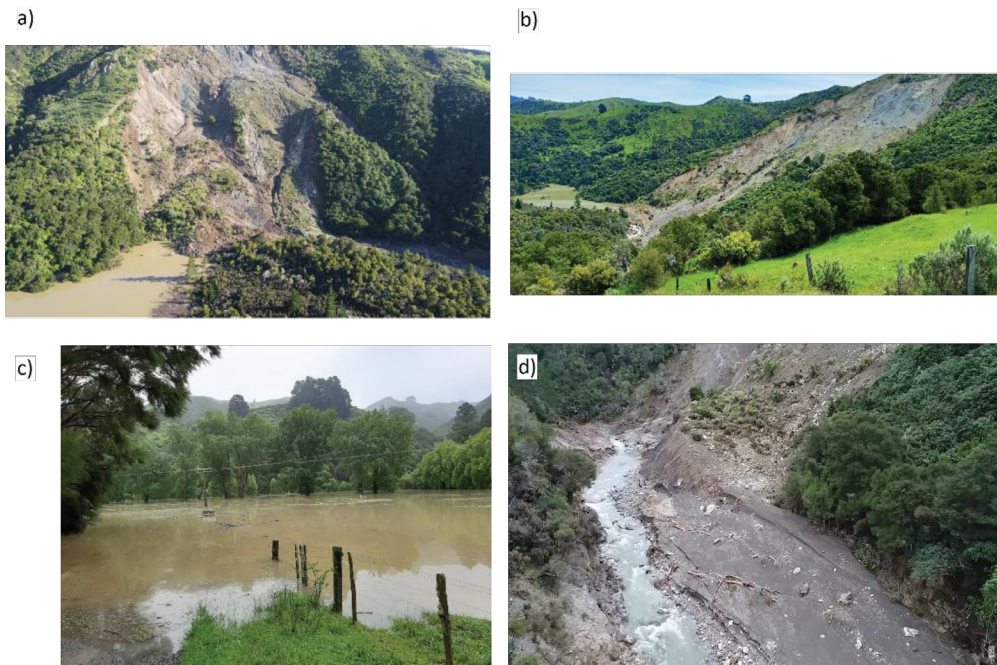**Figure 8. a) South-to-north view of the third landslide failure (photograph: © M. Anselm); b) Landslide formed a dam and blocked the river; the landslide-dammed lake is visible on the left side (photograph: © Lithofile); c) Lake was formed upstream and flooded the land and infrastructure (photograph: © M. Anselm); d) Dam failed and enormous amount of water went downstream (photograph: © GNS).**

3.2 Data

3.2.1 Optical Satellite Data

In this study, a time series of Sentinel-2 images were used with 10 m spatial resolution derived by European Union's Earth Observation programme, Copernicus. Sentinel-2 has provided available optical multi-spectral data with 13 spectral bands and different spatial resolutions (up to 10 m for Red, Green, Blue (RGB) and Near-infrared (NIR) bands) with the repeat cycle of 5 days (Drusch et al., 2012). The images were downloaded from Copernicus Open Access Hub[6], providing free and open access to Sentinel-2 data worldwide through Open Hub Graphical User Interface (GUI).

In addition, one PlanetScope satellite image, provided by Planet[7], with four spectral bands (RGB and NIR) and 3 m spatial resolution was used (Table 2). The reason behind this decision was due to the unavailable image with low cloud coverage by Sentinel-2 to capture the significant changes in the desired date (between 1st and 13th of June 2019).

The satellite images used in this study cover a series of Kaiwhata landslide events and evolutions from 2017 to 2021. The images were selected based on visual inspection, where changes could be recognised compared to the previous date and considering cloud coverage. In addition, Morgenstern et al. (2021) highlighted two important dates regarding the initial and second landslide failures.

Table 2. Satellite Images used for the analysis

Sensor, Product	Date	Event Description
Sentinel-2B MSI, Level 1-C	13 October 2017	First Landslide Failure
Sentinel-2B MSI, Level 1-C	16 January 2018	
Sentinel-2A MSI, Level 1-C	13 September 2018	
Sentinel-2A MSI, Level 1-C	12 November 2018	
PlanetScope MSI	8 June 2019	Second Landslide Failure
Sentinel-2A MSI, Level 1-C	18 September 2019	
Sentinel-2B MSI, Level 1-C	12 December 2019	
Sentinel-2A MSI, Level 1-C	11 November 2020	Third Landslide Failure
Sentinel-2A MSI, Level 1-C	1 December 2020	
Sentinel-2B MSI, Level 1-C	15 January 2021	

3.2.2 Topographic Data

The Land Information New Zealand (LINZ)[8] Data Service provides topographic and cadastral data and information in different categories that are accessible to the public. Through this platform, The Wellington region DEM data were acquired with 1 m spatial resolution, derived from LiDAR data between 2013 and 2014. Although the available data do not cover the overall period of interest, the DEM and its derivatives, such as slope and aspect, were inserted as auxiliary data and helped to distinguish landslide and landslide-dammed lake areas from other areas. The DEM data were also crucial in the 3D visualization step to illustrate the results through static and interactive models.

---

[6] https://scihub.copernicus.eu/
[7] https://www.planet.com/explorer/
[8] https://www.linz.govt.nz/

In addition, the main vector datasets of the area of interest were needed to illustrate the main affected areas during the evolution of the Kaiwhata landslide. They include buildings, Kaiwhata road, power line, and croplands.

3.3 Software

The main data analysis step was applied in **Trimble eCognition Developer 10.3**. The software helped to apply object-based image analysis by developing set of knowledge-based rule sets to semi-automatically map the landslide and landslide-dammed lake.

ArcGIS Pro 3.0.2 was used to do the accuracy assessment of the results. In addition, it was used to provide 3D static models of results to illustrate the evolution of the events on the textured 3D surface for better understanding of the changes.

Qgis Desktop 3.26.2 was used to provide 2D static maps to show the results of the applied OBIA methodology. In addition, the author used the added-in plugin called Qgis2threejs in Qgis desktop environment for the 3D web model of the results.

Qgis2threejs is a Python plugin of Qgis that utilizes three.js library, which facilitates exporting terrain data, map canvas images, and vector data to browsers that support the WebGL. It was used to utilize its capability of exporting the results to a 3D visualization model as HTML files, which can be easily embedded in websites. This feature made it a useful tool for creating interactive 3D web model to visualize the results.

Microsoft Visual Studio 2022 as an integrated development environment (IDE) was used to edit the cascading style sheets (CSS) of the exported 3D web model from Qgis2threejs plugin to provide a more legible interface to the user.

Adobe Illustrator 2020 as a vector graphics editor was used to edit the static 3D models of the landslide failures to show their changes in time.

3.4 Workflow

Figure (9) shows the workflow of this study. The procedure starts from the data acquisition through different services and filter the images based on cloud coverage and their availability in a desired date. Applying image analysis based on OBIA methodology to modify a single workflow for delineating landslide failures and landslide-dammed lakes, the results were followed up by an accuracy assessment to compare the OBIA mapped outputs with manual mapping. The visualization of the results in 2D and 3D were provided to reflect the changes and the evolution of failures into static and interactive ways.
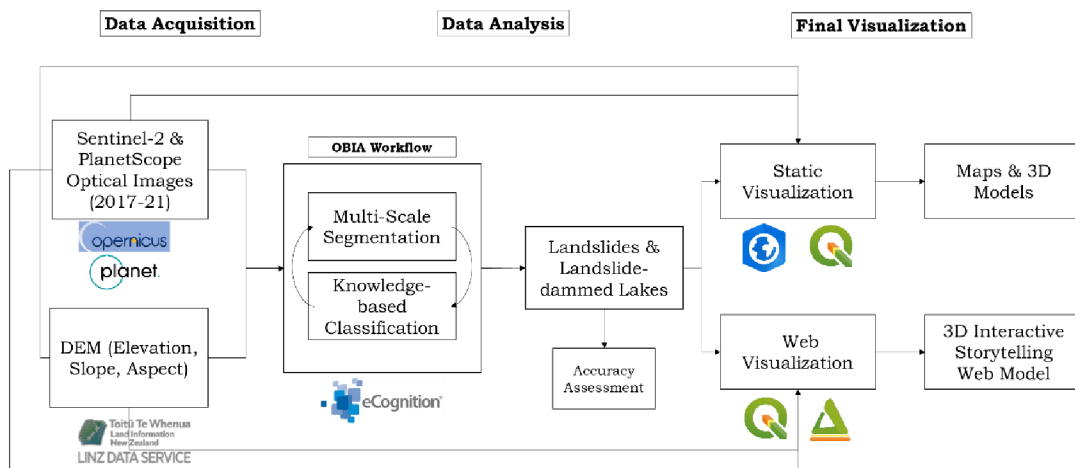

Figure 9. Thesis Workflow

4 ANALYSIS PROCEDURE

This chapter explains the steps and the achievements of the data acquisition and analysis, based on the workflow that was discussed in section 3.4.

4.1 Data Acquisition

This section highlights the process of acquiring the main data needed for this study. The main data include satellite imagery data and topographic data that were acquired taking into consideration the acquisition time, the area of interest, and spatial resolution.

4.1.1 Acquisition of Sentinel-2 imagery from Open Access Hub

The Copernicus Sentinel programme is a European Union Earth Observation programme that aims to provide an extensive range of data and images of the Earth's surface, oceans, and atmosphere. The programme utilizes a constellation of satellites, known as Sentinels, to capture high-resolution data, which can be used for a range of applications. Sentinel-2 provides high-resolution images (10 m, 20 m, 60 m) with 13 spectral bands for monitoring and managing land and vegetation.

The data is accessible through Copernicus Open Access Hub (https://scihub.copernicus.eu/). It is an online platform that provides free and open access to the data collected by the Sentinel satellites. The platform allows users to search, view, and download data from the Sentinel missions, including Sentinel-2. The data can be accessed through a web-based interface or via an API, which enables users to automate data retrieval and processing.

The steps below explains the procedure to acquire imagery data from Open Access Hub. Figure (10 & 11) show the steps as follow:

i. Open Hub is the interactive web-based interface to access the data;
ii. The user needs to create an account to log into the portal;
iii. The area of interest needs to be defined by drawing a rectangle in the area of interest;
iv. The sensing period (date) and imagery type (sentinel-2) were defined in the search section;
v. Available images were listed and the final selection was based on the minimal cloud cover. In addition, Level-1C processing level was selected for the images; which is orthorectified and includes geometric and radiometric corrections to the raw data.
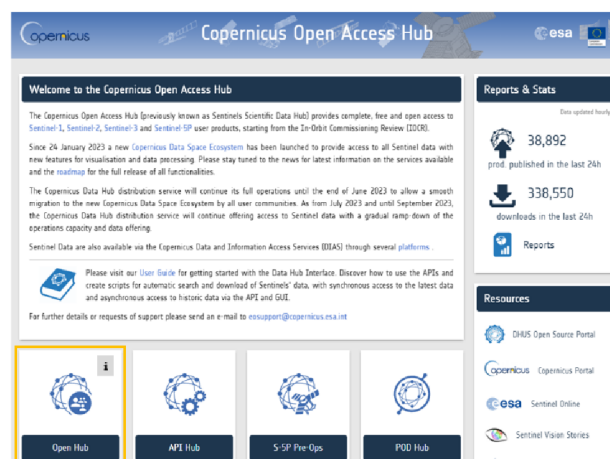

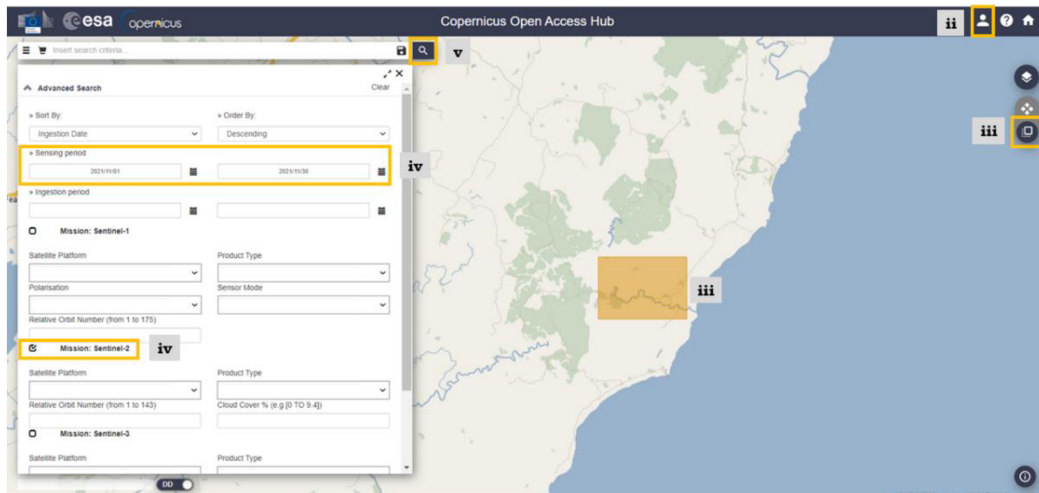**Figure 10. The homepage of Copernicus Open Access Hub**

Figure 11. Copernicus Open Hub interface

4.1.2 Acquisition of PlanetScope Imagery from Planet Explorer

In order to monitor the evolution of the landslide failure and the following significant changes, PlanetScope image was used to fill the gap between 1st and 13th of June 2019. The available images from Sentinel-2 in this period were accompanied by high cloud coverage and therefore, using PlanetScope helped to capture the significant change during the mentioned period. Planet's satellites capture images of the Earth's surface at high frequency and resolution, allowing for near-real-time monitoring of changes in the environment. One of the key products offered by Planet is PlanetScope imagery, which provides high-resolution images of the Earth's surface with an average revisit time of one to three days.

Even though Planet is a commercial satellite imagery provider, the company offers "Education and Research Programme" service that supports students and researchers to access PlanetScope and RapidEye data, limited to 5,000 km^2 per month.

Planet Explorer (https://www.planet.com/explorer/) interface was used to access the required image. The steps below explains the procedure to acquire imagery data from Planet Explorer. Figure (12) shows the steps as follow:

i. User needs to register an account for students and researchers[9] and log in,

ii. It is possible to search the location of the area of interest. By doing that, a rectangle will be drawn automatically as the area of interest. It is also possible to draw the rectangle manually for more accurate delineation,

iii. Filter provides the options to choose the required spectral bands beside RGB bands such as near-infrared band (NIR), to define the cloud coverage, and etc. The desired period is defined through Dates,

iv. After defining the desired period, the engine provides the list of available images. It is possible now to preview the image and also to order the image for downloading.
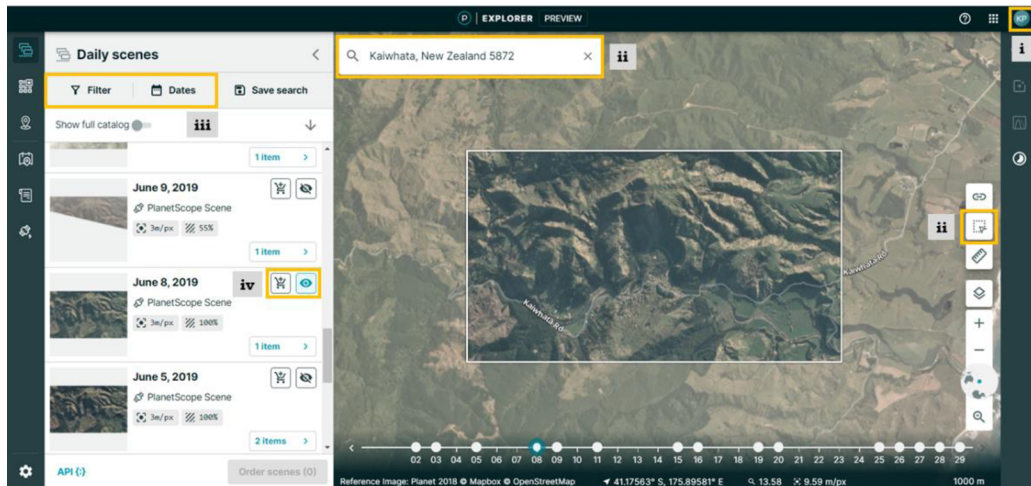
---

[9] https://www.planet.com/markets/education-and-research/

Figure 12. Planet Explorer interface

4.1.3 Acquisition of Topographic Data from LINZ Data Service

In order to acquire reliable data for this study, Land Information New Zealand (LINZ) data service was used to access to a wide range of geospatial and cadastral data for New Zealand. In general, The platform hosts a vast array of data sets, including topographic maps, aerial imagery, cadastral data, elevation models, land cover data, and other geospatial data. The data can be accessed through a web-based interface. The steps below explains the procedure to acquire the necessary data from LINZ data service. Figure (13) shows the steps as follow:

   i.   The user needs to create an account in order to use the services,

   ii.   For the better visualization of the data, the area of interest should be searched,

  iii.   The keywords related to the necessary data was searched and a list of results was provided by the engine. After browsing among the results, the data were selected,

  iv.   By drawing a rectangle, the data were clipped to export based on the area of interest. The data were ready to download at the end.
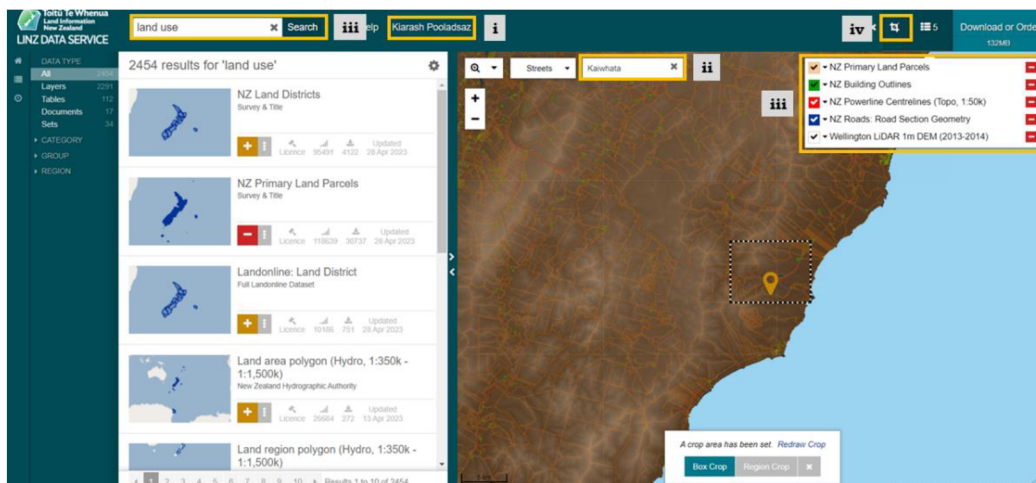
Figure 13. LINZ Data Service Interface (Source: https://data.linz.govt.nz/)

4.2 Data Processing & Analysis

After acquiring the necessary data for this study, the satellite images and the DEM data were imported to Trimble eCognition software to initialize the image analysis. The

24

first part mentions the required layers and indices that were essential for the data analysis. The second part identifies the type of segmentation and the main parameters and layers that were considered to apply the segmentation. The third part addresses the knowledge-based classification parameters that helped to semi-automatically map and monitor landslide and landslide-dammed lake classes. The last part provides the overall OBIA workflow that was applied to the data input to capture the desired classes.

Trimble eCognition[10] is being recognised for object-based image analysis. It functions to add value to pixel information in iterative segmentation and classification steps to extract the knowledge in a semantic network. It follows the human mind, combining the colour, shape, texture, and size of objects as well as their relationships and context. The object classification could be based on knowledge-based, fuzz logic and machine learning and proceed into a ruleset. The rule set is the output of translating the mind models into computer understandable code. Figure (14) shows the workspace of the software.
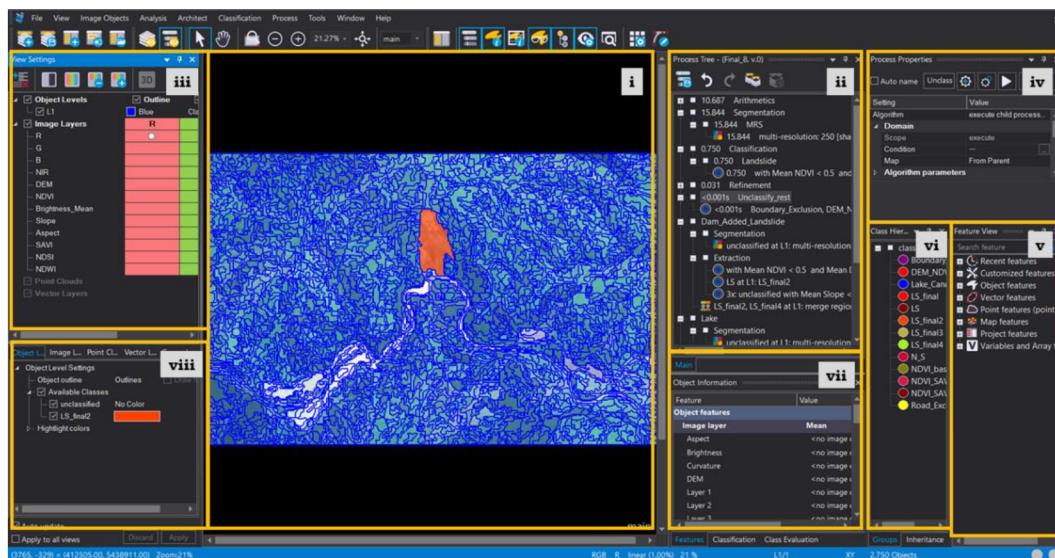

Figure 14. eCognition Workspace; i) Main View, ii) Process Tree, iii) View Settings, iv) Process Properties, v) Feature View, vi) Class Hierarchy, vii) Object Information, viii) Layer Settings.

The main approach to analyse the input data was followed by an iterative cycle of trial and error. The values adopted during the analysis were the result of this approach. It followed multi-scale segmentation and knowledge-based classification rules to semi-automatically map landslide and landslide-dammed lake classes on each image. The semi-automatic approach combined automated image analysis and manual input; e.g. it involved manual refinements in segmentation and providing input (e.g., features and thresholds) for classification. The classification rules and parameters were developed from the first image to the subsequent ones, following the evolution of the landslide and the landslide-dammed lake area. Therefore, the modified ruleset consist of input layers, (multi-scale) segmentation, classification and refinement of previous image was applied to the next image analyses and was evolved if necessary.

---

[10] https://geospatial.trimble.com/what-is-ecognition

4.2.1 Image Layers Preparation

Spectral indices and terrain data took the main role of the OBIA approach. In addition to the available red, green, blue, and near-infrared bands besides the DEM data, Table (3) provides the list of indices and terrain data that were applied to the image analysis. These layers were calculated in eCognition environment with the set of rules.

Table 3. Input Calculated Layers for OBIA

Input Layers	Description	Calculation
Pixel Brightness	the amount of light reflected or emitted by a single pixel	$\dfrac{(\text{Red} + \text{Green} + \text{Blue})}{3}$
NDVI	Normalized Difference Vegetation Index	$\dfrac{(\text{NIR} - \text{Red})}{(\text{NIR} + \text{Red})}$
NDWI	Normalized Difference Water Index	$\dfrac{(\text{Green} - \text{NIR})}{(\text{Green} + \text{NIR})}$
SAVI[11]	Soil Adjusted Vegetation Index	$\left(\dfrac{(\text{NIR} - \text{Red})}{(\text{NIR} + \text{Red} + L^{12})}\right) * (1 + L)$
Slope	measure of the steepness of the terrain	Zevenburgen & Thorne (1987) algorithm in eCognition
Aspect	direction that a slope faces	Horn's method (1981) algorithm in eCognition

The input layer calculations were executed using Layer Arithmetics, Index Layer Calculation, and Surface Calculation algorithms that were defined in process tree (Figure 15). It must be reminded that not all the images were needed the whole calculated layers for the analysis and the requirements for more layers increased during the evolution of the landslide. Figure 16 shows the values of each layer within the area of interest. Sentinel-2 image from 11 November 2020 was selected as an example to show values of input layers.
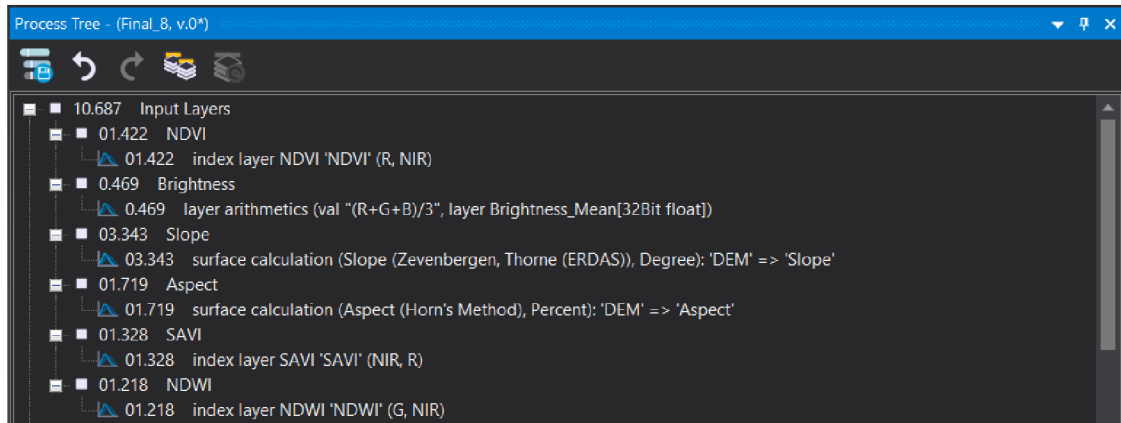

Figure 15. Input layers calculation defined in process tree

---

[11] Calculated only for the PlanetScope imagery
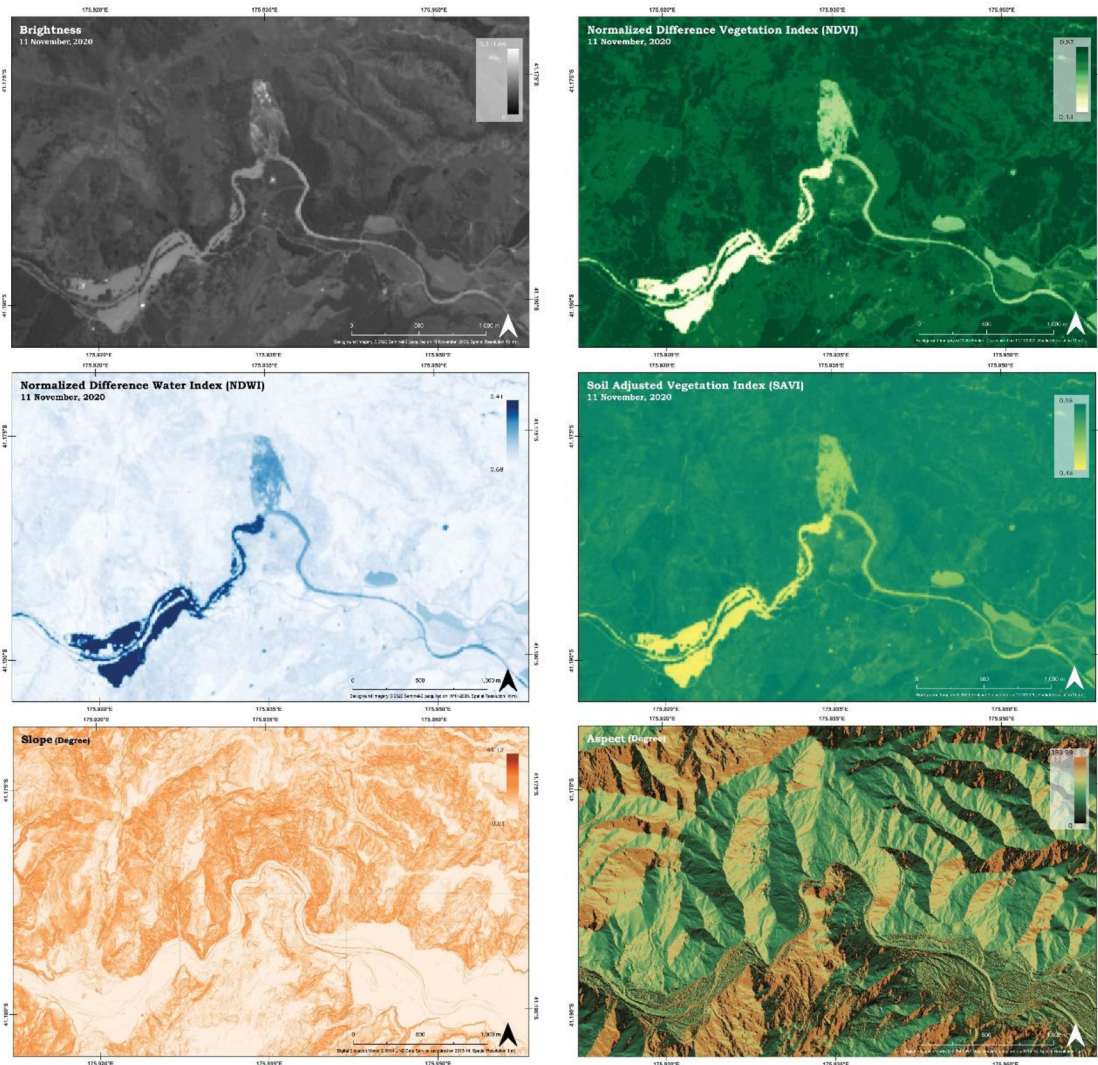[12] Soil brightness correction factor

Figure 16. Calculated Input Layers (Sentinel-2, 11 November 2020)

4.2.2 Multi-scale Segmentation

Researches mentioned the efficiency of Multiresolution Segmentation (MRS) in landslide mapping (Table 1). The concept presented by Battz & Schape (2000), minimizes the average heterogeneity of image objects considering the resolution of the image. It follows an iterative bottom-up approach, whereby objects are grouped until a threshold representing the upper object variance is reached. The algorithm maximizes the average homogeneity (variance threshold) of objects, where the homogeneity criterion is defined as the combination of shape and compactness criteria in eCognition to minimize the fractal borders of the object:

i.   Shape criterion value modifies the relationship between shape and colour;
ii. Compactness criterion weighs the compactness of the objects that are formed during the segmentation.

In addition to these criteria, scale parameter is another factor that determines the maximum allowed heterogeneity for the resulting image objects. It controls the amount of spectral variation within objects. The user also identifies the main layers that should be considered in segmentation. Figure (17) shows the eCognition environment to apply the MRS algorithm.
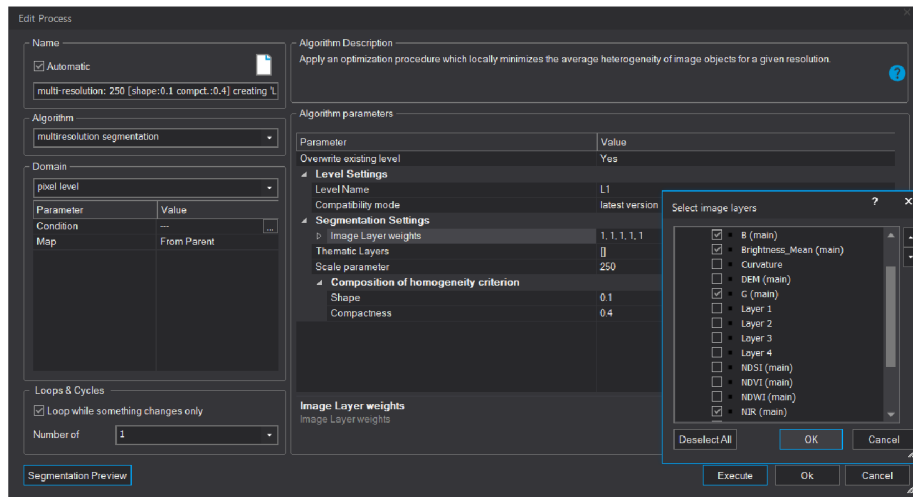
27

Figure 17. Multiresolution Segmentation Algorithm in eCognition

In order to modify a single workflow for the OBIA approach to apply equally on all the images, different sets of values were adopted to the segmentation parameters. Drăguț et al. (2010) introduce ESP tool to automatically estimate the scale parameter value for image segmentation. However, due to the multiplicity of images, it was decided to assign values based on several tests and visual interpretations.

For segmentation of the landslide area, the four multispectral bands, the NDVI, and the brightness layer were used. However, the landslide reached the Kaiwhata River in June 2019 (Figure 7), and it was challenging to distinguish the landslide from the riverbed. Since the characteristics of the deposition zone of the landslide area and the riverbed were similar, another MRS was to create homogeneous objects based on NDWI and NDVI indices that helped us to better map the total landslide area. Another MRS was applied to detect the landslide-dammed lake area based on the NDWI, the DEM, and the slope. Table (4) provides information about the parameters and layers assigned for each image's multi-scale segmentation.

Table 4. Multi-Scale MRS description

Event Description	Data	Class	Parameters for Multiresolution Segmentation	Layers for Segmentation
First Landslide Activity	Sentinel-2 (13 October 2017; 16 January 2018; 13 September 2018; 12 November 2018)	Landslide	Scale Parameter: 250; Shape criterion: 0.1; Compactness criterion: 0.4	blue, green, red, NIR, brightness
Second Landslide Activity	PlanetScope (8 June 2019)	Landslide	Scale Parameter: 50; Shape criterion: 0.3; Compactness criterion: 0.6	blue, green, red, NIR, brightness, NDVI, SAVI
		Landslide-dammed Lake	Scale Parameter: 25; Shape criterion: 0.1; Compactness criterion: 0.4	NDWI, DEM, slope

28

	Sentinel-2 (18 September 2019; 12 December 2019))	Landslide	First part: Scale Parameter: 250; Shape criterion: 0.1; Compactness criterion: 0.4	blue, green, red, NIR, brightness
			Second part: Scale Parameter: 10; Shape criterion: 0.1; Compactness criterion: 0.4	NDVI, NDWI
Third Landslide Activity	Sentinel-2 (11 November 2020; 1 December 2020; 15 January 2021)	Landslide	First part: Scale Parameter: 250; Shape criterion: 0.1; Compactness criterion: 0.4	blue, green, red, NIR, brightness
			Second part: Scale Parameter: 10; Shape criterion: 0.1; Compactness criterion: 0.4	NDVI, NDWI
		Landslide-dammed Lake	Scale Parameter: 10; Shape criterion: 0.1; Compactness criterion: 0.4	NDWI, DEM, slope

The spatial resolution of PlanetScope satellite image influenced the values dedicated to segmentation parameters. In addition, due to the morphologic characteristics of the study area during the summer, the landslide was covered by shadow. Therefore, NDVI and SAVI indices were also added for MRS dedicated to landslide. Other images followed the same procedure to modify a unique workflow for the analysis. Figure (18) shows an example of multi-scale MRS applied to Sentinel-2 image (11 November 2020). The first segmentation was followed by knowledge-based classification and then only unclassified objects were taken for the second segmentation and classification. This procedure was applied to the third step as well.
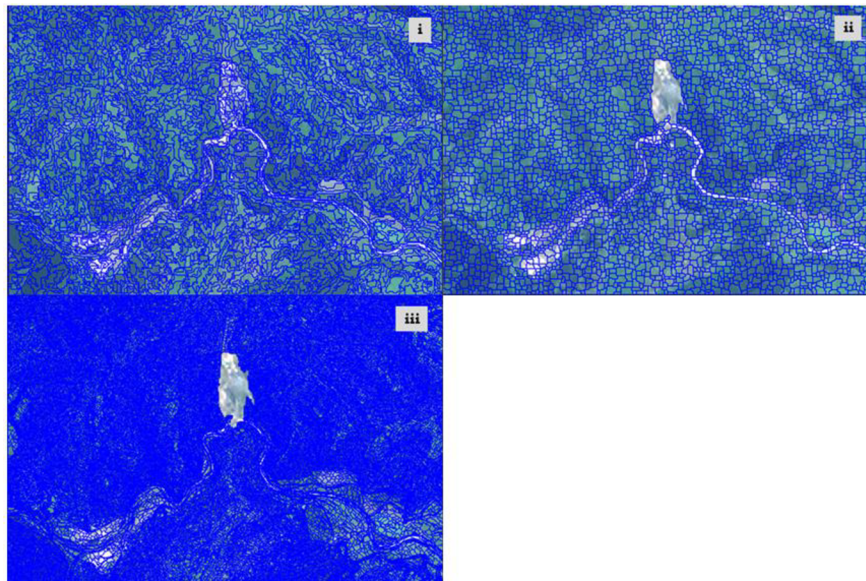

Figure 18. MRS on Sentinel-2 image (11 November 2020); i) SP: 250, shape: 0.1, compactness: 0.4, Layers: B, G, R, NIR, mean brightness, ii) SP: 10, shape: 0.1, compactness: 0.4, Layers: NDVI, NDWI, iii) SP: 10, shape: 0.1, compactness: 0.4, Layers: NDWI, DEM, slope.

Unclassified objects were taken into each step of MRS. The first MRS was applied to pixel level (Sentinel-2 image), the second and third MRS were applied to object level and unclassified objects were taken to apply the second and third segmentations. To understand the workflow effectively, Figure 19 shows the workflow that was applied to Sentinel-2 image from 11 November 2020. This image was selected as an example to show the complete segmentation workflow. The first step was applied to all Sentinel-2 images, while the second step was applied to Sentinel-2 images in second and third landslide activities. The third step was dedicated to map landslide-dammed lake.
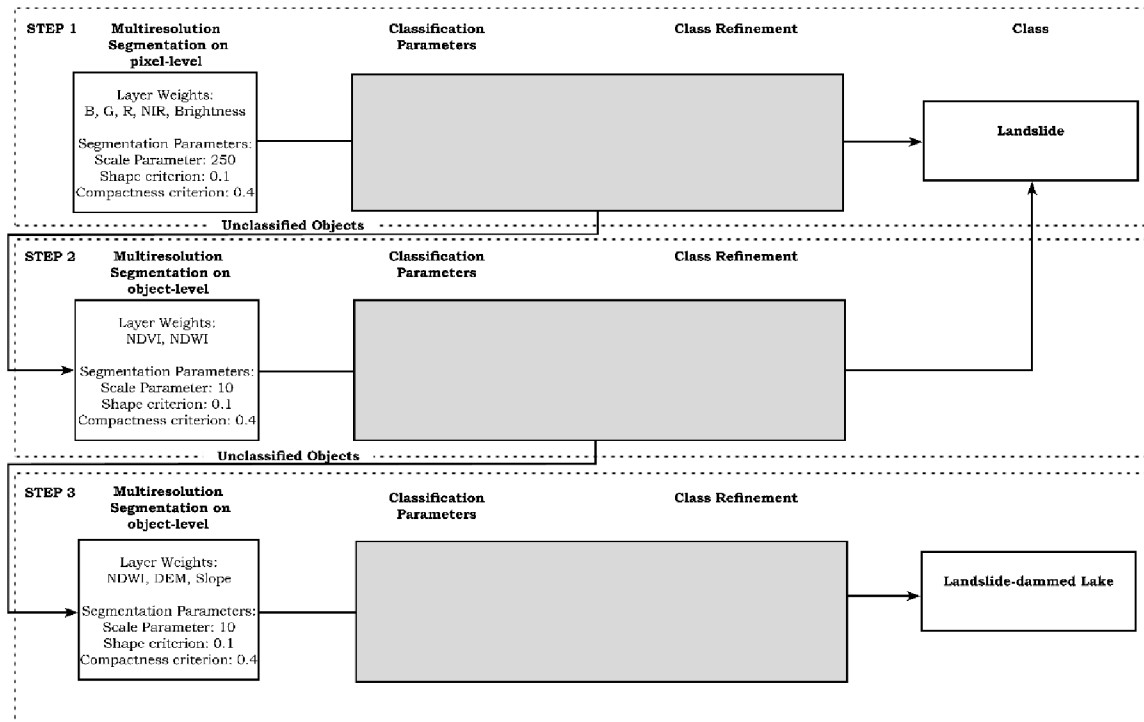

Figure 19. Multi-scale MRS workflow for Sentinel-2 image (11 November 2020). In addition, Step 1 was applied to all Sentinel-2 images; Step 2 was applied to second and third landslide activities; Step 3 was applied to PlanetScope image from second landslide activity and Sentinel-2 images from third landslide activity. The values were different for PlanetScope image (Table 4).

4.2.3 Classification Parameters

Image classification was initiated from the first image after the multiresolution segmentation and set of parameters were defined to classify the objects into the desired classes. The ruleset was expanded as the landslide evolved and therefore, more parameters were included during the classification. The classification was applied based on knowledge-based classification approach. This approach relies on a set of rules or a knowledge base to classify objects into different categories. This method is based on the idea that the specific class involves unique spectral, spatial, and contextual features that can be used to distinguish them from the other objects. The procedure includes identifying these features and then creating a set of rules that assign these features to a specific class.

The classification workflow initiated by set of parameters for Sentinel-2 image on 13 October 2017. Based on the object information, the classification was modified by defining "if" structure (assign class) as:

If NDVI < 0.5 AND

DEM > 200: Unclassified objects → Landslide Candidates.

Figure (20) shows the 2D feature space defined by NDVI (y axis) and DEM (x axis) and landslide candidate objects. It illustrates how these objects were distinguished from other unclassified objects when applying the classification rules. The illustration is based on two parameter, NDVI and DEM as y and x axis. As the ruleset was expanded over time, more parameters were involved and therefore, an illustrative feature space where the number of dimensions follows the multiplicity of involved classification parameters was shaped to distinguish the desired classes from unclassified objects.
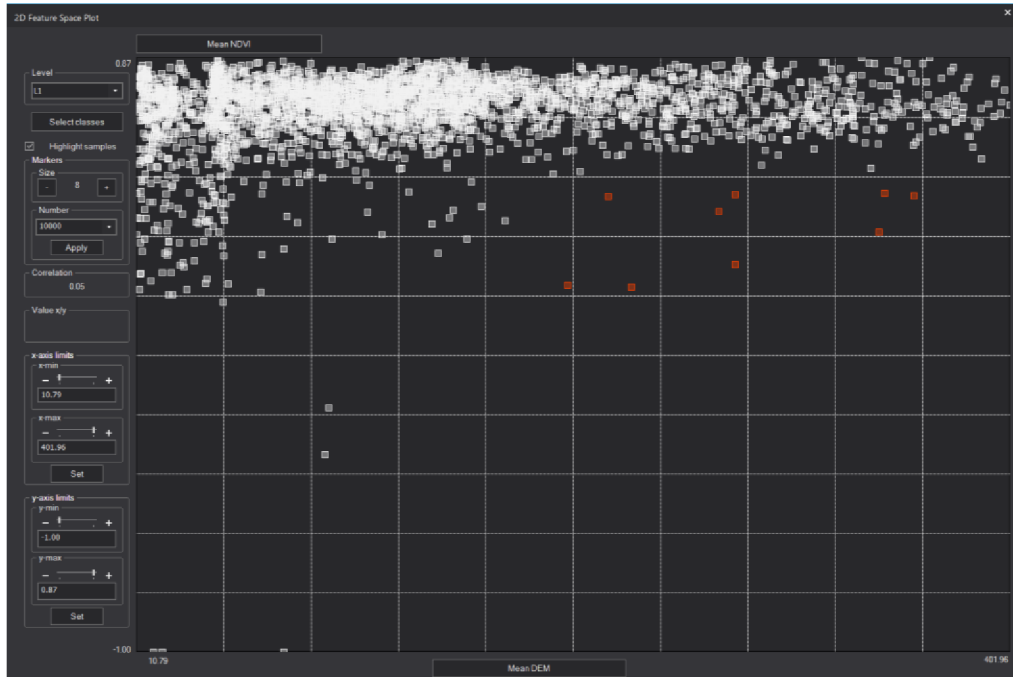

Figure 20. 2D feature space plot to show the objects distribution based NDVI and DEM values related to Sentinel-2 image (13. 10. 2017). Orange squares are landslide candidate objects.
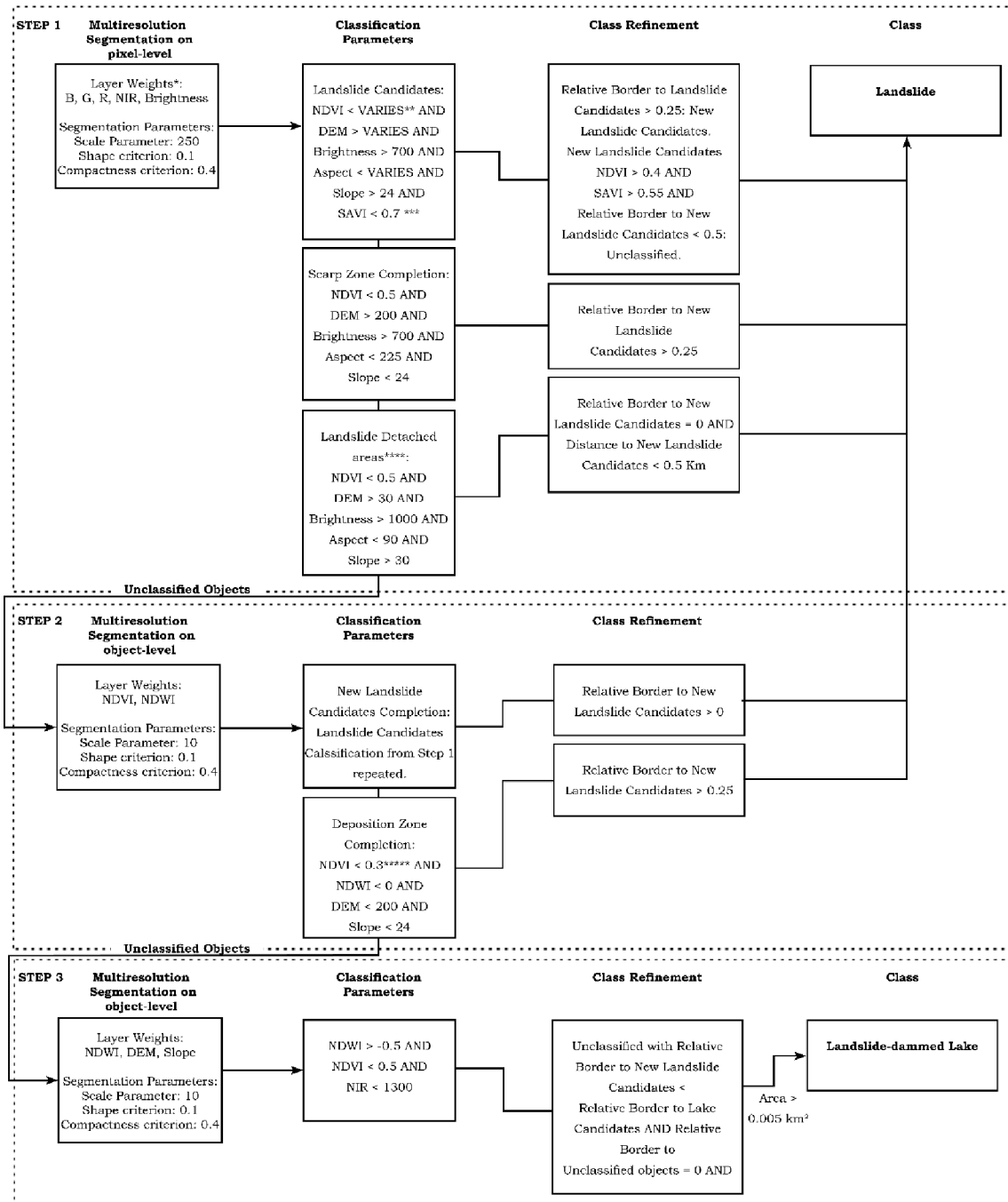
As mentioned earlier, the knowledge-based classification was mainly based on the calculated spectral indices. The main feature of the landslide area was the absence of vegetation, where landslide-affected areas can be distinguished from their surroundings by applying spectral indices, such as NDVI and the brightness layer. In addition, relatively low NDWI value was applied to distinguish the deposition area of the landslide from the riverbed. To map the landslide-dammed lake area, relatively low near-infrared and NDVI values, and higher NDWI values were considered for the final extraction. The DEM and its derivatives were used as auxiliary data to avoid the classification of false positives, for example, to distinguish the landslide area from the riverbed. The values for the classification parameters were assigned based on expert knowledge, information from the literature considering other related researches, and trial and error. Table (5) shows the list of classification parameters and their values adopted to classify landslide and landslide-dammed lake.

31

Table 5. Segmentation and classification parameters used for object-based landslide and landslide-dammed lake mapping. Multi-scale MRS was applied to Sentinel-2 images from the second and third landslide activity.

Event Description	Data	Class	Parameters for Multiresolution Segmentation	Layers for Segmentation	Main Classification Parameters
First Landslide Activity	Sentinel-2 (13 October 2017)	Landslide	Scale Parameter: 250; Shape criterion: 0.1; Compactness criterion: 0.4	blue, green, red, NIR, brightness	NDVI < 0.5 DEM > 200
	Sentinel-2 (16 January 2018)	Landslide	Scale Parameter: 250; Shape criterion: 0.1; Compactness criterion: 0.4	blue, green, red, NIR, brightness	NDVI < 0.45 DEM > 195
	Sentinel-2 (13 September 2018)	Landslide	Scale Parameter: 250; Shape criterion: 0.1; Compactness criterion: 0.4	blue, green, red, NIR, brightness	NDVI < 0.45 DEM > 195 Slope > 24 Aspect < 185
	Sentinel-2 (12 November 2018)	Landslide	Scale Parameter: 250; Shape criterion: 0.1; Compactness criterion: 0.4	blue, green, red, NIR, brightness	First Part: NDVI < 0.5 DEM > 190 Second Part: NDVI < 0.5 Mean Slope > 30 DEM > 30 Mean Aspect < 190 Relative Border First Border = 0 Mean Brightness > 1000 Distance to First Part < 0.5 km
Second Landslide Activity	PlanetScope (8 June 2019)	Landslide	Scale Parameter: 50; Shape criterion: 0.3; Compactness criterion: 0.6	blue, green, red, NIR, brightness, NDVI, SAVI	NDVI < 0.5 DEM > 30 Slope > 24 Aspect < 201 SAVI < 0.7
		Landslide-dammed Lake	Scale Parameter: 25; Shape criterion: 0.1; Compactness criterion: 0.4	NDWI, DEM, slope	NDVI < 0.5 NIR < 1300 NDWI > -0.5
	Sentinel-2 (18 September 2019)	Landslide	First part: Scale Parameter: 250; Shape criterion: 0.1; Compactness criterion: 0.4	blue, green, red, NIR, brightness	NDVI < 0.5 DEM > 30 Slope > 24 Aspect < 201 Mean Brightness > 700
			Second part: Scale Parameter: 10; Shape criterion: 0.1; Compactness criterion: 0.4	NDVI, NDWI	NDVI < 0.3 NDWI < 0 Slope < 24 DEM < 200 Relative Border to First part > 0.25

	Sentinel-2 (12 December 2019)	Landslide	First part: Scale Parameter: 250; Shape criterion: 0.1; Compactness criterion: 0.4	blue, green, red, NIR, brightness	NDVI < 0.5 DEM > 30 Slope > 24 Aspect < 225 Mean Brightness > 700
			Second part: Scale Parameter: 10; Shape criterion: 0.1; Compactness criterion: 0.4	NDVI, NDWI	NDVI < 0.3 NDWI < 0 Slope < 24 DEM < 200 Relative Border to First part > 0.25
Third Landslide Activity	Sentinel-2 (11 November 2020; 1 December 2020; 15 January 2021)	Landslide	First part: Scale Parameter: 250; Shape criterion: 0.1; Compactness criterion: 0.4	blue, green, red, NIR, brightness	NDVI < 0.5 DEM > 30 Slope > 24 Aspect < 225 Mean Brightness > 700
			Second part: Scale Parameter: 10; Shape criterion: 0.1; Compactness criterion: 0.4	NDVI, NDWI	NDVI < 0.3 NDWI < 0 Slope < 24 DEM < 200 Relative Border to First part > 0.25
		Landslide-dammed Lake	Scale Parameter: 10; Shape criterion: 0.1; Compactness criterion: 0.4	NDWI, DEM, slope	NDVI < 0.5 NIR < 1300 NDWI > -0.5

Figure (21) shows the overall framework of landslide and landslide-dammed lake classification. The ruleset follows several steps to assign the desired classes. Each step consist of multiresolution segmentation, set of classification parameters, and class refinement. Meanwhile, this overall workflow was not applied to all the images, where the evolution of the landslide failure was accompanied by more sets of parameters and refinements. The values dedicated to some layers such as NDVI, DEM, and aspect were varied (VARIES) due to seasonal changes and morphological evolution of the landslide. The second step helped to distinguish the deposition zone of the landslide from the riverbed to complete the extent of the landslide. The difficulty stemmed from the texture similarity between them and applying multiresolution segmentation on the unclassified objects from the first step helped to identify the remained landslide area effectively. DEM and slope were effective layers for segmentation in the third step and NDWI, NDVI, and NIR indices were applied to extract landslide-dammed lake. Spatial features (e.g., relations to neighbour objects) had key role in the classification refinement besides spectral indices.

STEP 1

Multiresolution Segmentation on pixel-level

Classification Parameters

Class Refinement

Class

Layer Weights*:
B, G, R, NIR, Brightness

Segmentation Parameters:
Scale Parameter: 250
Shape criterion: 0.1
Compactness criterion: 0.4

Landslide Candidates:
NDVI < VARIES** AND
DEM > VARIES AND
Brightness > 700 AND
Aspect < VARIES AND
Slope > 24 AND
SAVI < 0.7 ***

Relative Border to Landslide
Candidates > 0.25: New
Landslide Candidates.
New Landslide Candidates
NDVI > 0.4 AND
SAVI > 0.55 AND
Relative Border to New
Landslide Candidates < 0.5:
Unclassified.

Landslide

Scarp Zone Completion:
NDVI < 0.5 AND
DEM > 200 AND
Brightness > 700 AND
Aspect < 225 AND
Slope < 24

Relative Border to New
Landslide
Candidates > 0.25

Landslide Detached
areas****:
NDVI < 0.5 AND
DEM > 30 AND
Brightness > 1000 AND
Aspect < 90 AND
Slope > 30

Relative Border to New
Landslide Candidates = 0 AND
Distance to New Landslide
Candidates < 0.5 Km

Unclassified Objects

STEP 2

Multiresolution Segmentation on object-level

Classification Parameters

Class Refinement

Layer Weights:
NDVI, NDWI

Segmentation Parameters:
Scale Parameter: 10
Shape criterion: 0.1
Compactness criterion: 0.4

New Landslide
Candidates Completion:
Landslide Candidates
Calssification from Step 1
repeated.

Relative Border to New
Landslide Candidates > 0

Relative Border to New
Landslide Candidates > 0.25

Deposition Zone
Completion:
NDVI < 0.3***** AND
NDWI < 0 AND
DEM < 200 AND
Slope < 24

Unclassified Objects

STEP 3

Multiresolution Segmentation on object-level

Classification Parameters

Class Refinement

Class

Layer Weights:
NDWI, DEM, Slope

Segmentation Parameters:
Scale Parameter: 10
Shape criterion: 0.1
Compactness criterion: 0.4

NDWI > -0.5 AND
NDVI < 0.5 AND
NIR < 1300

Unclassified with Relative
Border to New Landslide
Candidates <
Relative Border to Lake
Candidates AND Relative
Border to
Unclassified objects = 0 AND

Area >
0.005 km²

Landslide-dammed Lake

* The values are different for PlanetScope image (Table 5).   **VARIES refer to values that are available in Table 5.   *** SAVI has been used only for PlanetScope image.   **** Detached areas exist only in 12 November 2018.   ***** The value is 0.4 for image in 15 January 2021.

Figure 21. Overall OBIA workflow to monitor the evolution of the Kaiwhata landslide and the landslide-dammed lake

In order to enhance the procedural clarity and facilitate a comprehensive understanding of the main three steps involved, Sentinel-2 image from 11 November 2020 was selected with the intention of illustrating the procedure and details of the workflow clearly. The following Figures (22, 23, & 24) illustrate the result of each step from OBIA workflow that were applied on the mentioned Sentinel-2 image. The procedure followed the workflow from Figure 21 and the parameter values followed Table (5).

Step 1:

i. *Segmentation at pixel level. Layer weight: blue, green, red, NIR, Mean brightness; Scale Parameter: 250, Shape criterion: 0.1, Compactness criterion: 0.4.*

ii. *From Unclassified Objects, If NDVI < 0.5 AND DEM > 30 m AND Slope > 24° AND Aspect < 225[13] AND Mean Brightness > 700: Unclassified objects → Landslide Candidates.*

iii. *From Landslide Candidates, If Relative Border to Landslide Candidates > 0.25: Landslide Candidates → New Landslide Candidates.*

iv. *Scarp Zone Completion. From Unclassified Objects, If NDVI < 0.5 AND DEM > 200 AND Mean Brightness > 1000 AND Aspect < 90 AND Slope > 30° AND Relative Border to New Landslide Candidates > 0.25: Unclassified Objects → New Landslide Candidates.*
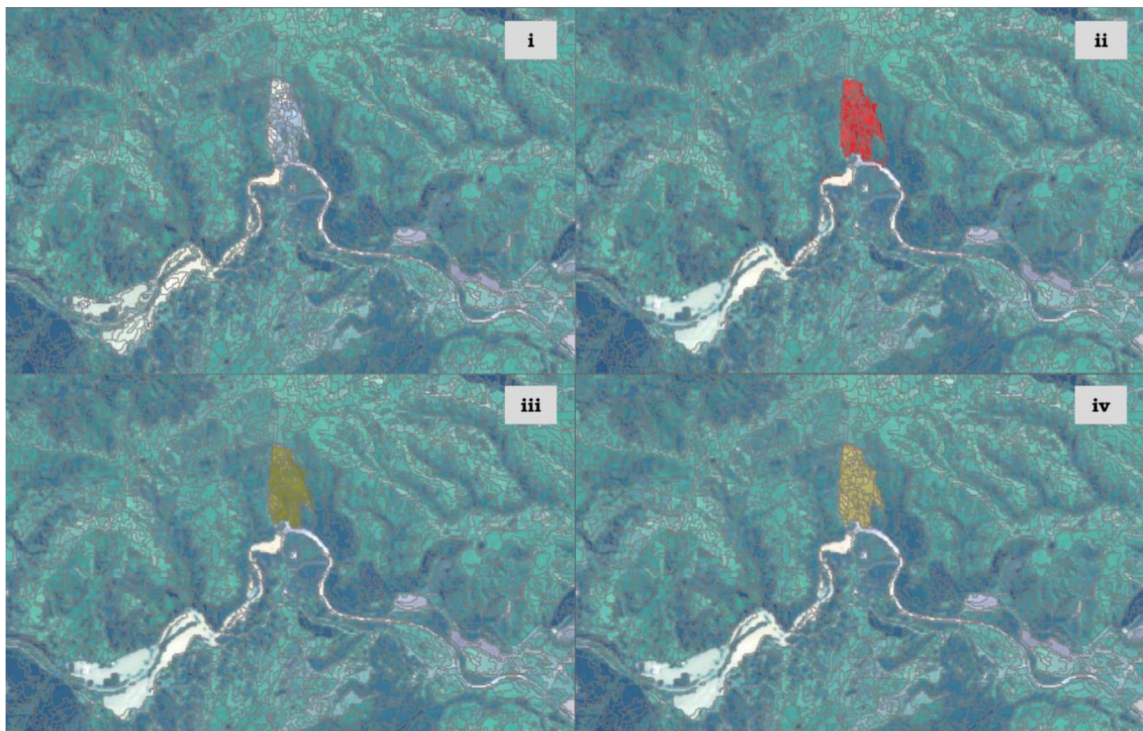
Figure 22. Applying first step of the workflow on Sentinel-2 image (11 November 2020).

Step 2:

v. *Segmentation at object level (only Unclassified Objects). Layer weight: NDVI, NDWI; Scale Parameter: 10; Shape criterion: 0.1; Compactness criterion: 0.4.*

vi. *From Unclassified Objects, If NDVI < 0.5 AND DEM > 30 AND Mean Brightness > 700 AND Aspect < 225 AND Slope > 30 °: Unclassified Objects → New Landslide Candidates.*

vii. *From New Landslide Candidates, If Relative Border to New Landslide Candidates = 0: New Landslide Candidates → Unclassified Objects.*

viii. *From Unclassified Objects, If Slope < 24 ° AND NDVI < 0.3 AND DEM < 200 AND NDWI < 0: Unclassified Objects → New Landslide Candidates (2).*

---

[13] *225 ° from north, which is south-west.*

ix. *From New Landslide Candidates (2), If Relative Border to New Landslide Candidates > 0.25: New Landslide Candidates (2) → New Landslide Candidates (3).*

x. *Assign and Merge New Landslide Candidates Objects with New Landslide Candidates (3) → **Landslide Class**.*
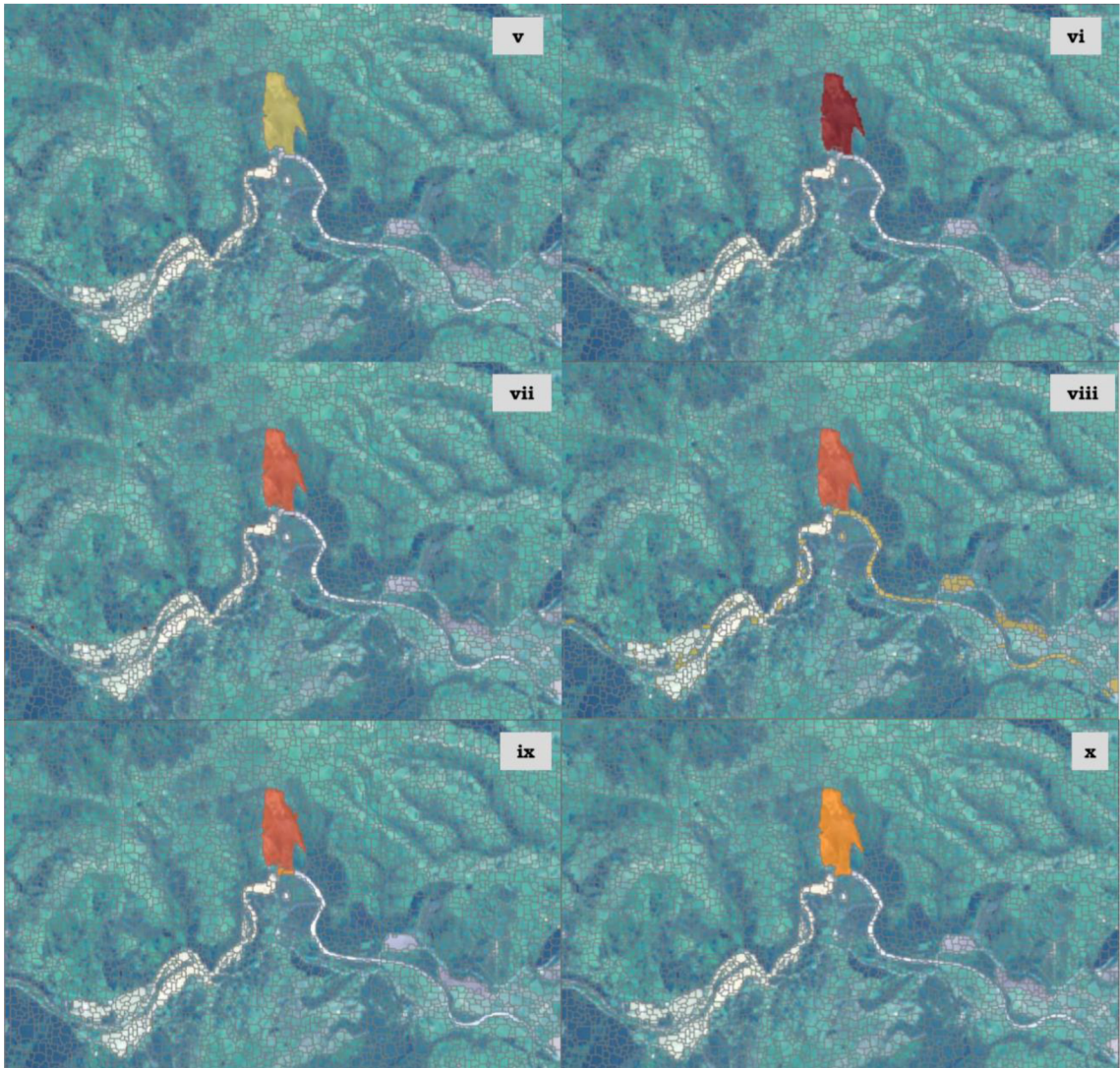

Figure 23. Applying second step of the workflow on Sentinel-2 image (11 November 2020).

Step 3:

xi. *Segmentation at object level (only Unclassified Objects). Layer weight: NDWI, DEM, Slope; Scale Parameter: 10; Shape criterion: 0.1; Compactness criterion: 0.4.*

xii. *From Unclassified Objects, If NDWI > -0.5 AND NDVI < 0.5 AND NIR < 1300: Unclassified → Landslide-dammed Candidates.*

xiii. *From Unclassified Objects, If Relative Border to Landslide-dammed Lake Candidates > Relative Border to Landslide AND Relative Border to Landslide > 0 AND Relative Border to Unclassified Objects = 0: Unclassified Objects → Landslide-dammed Lake Candidates.*

36

*From Landslide Dammed Lake Candidates, If Area > 0.005 km2: Landslide-dammed Lake Candidates → **Landslide-dammed Lake Class**.*
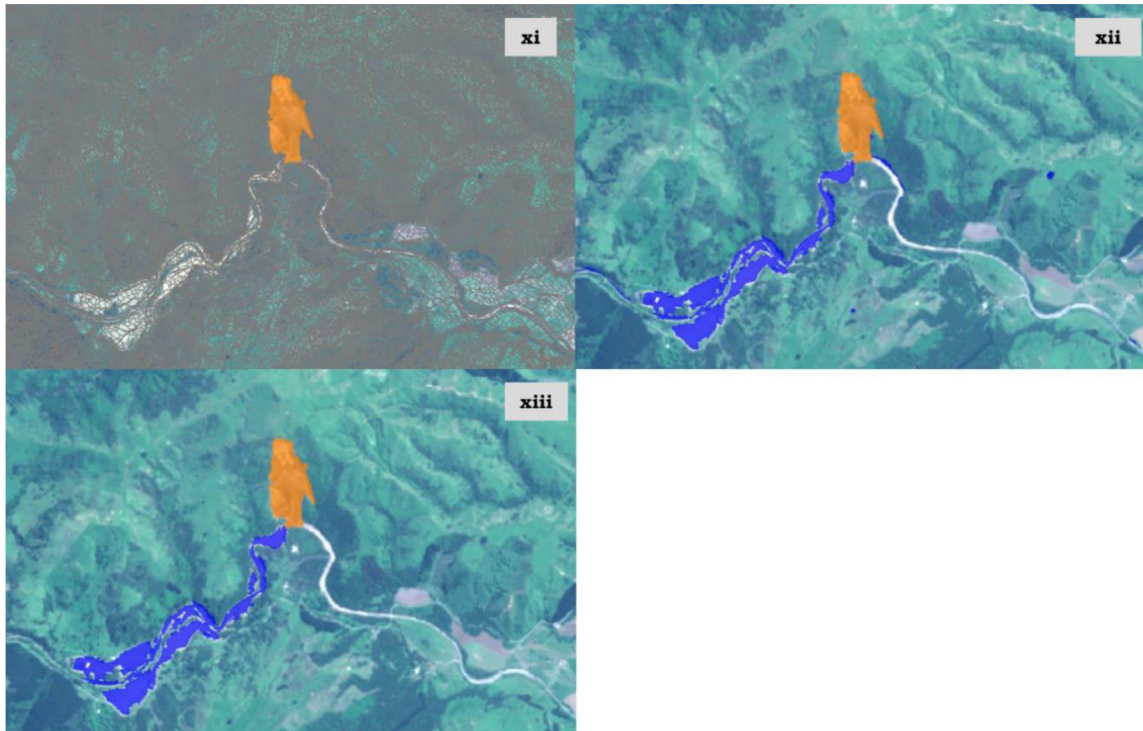
Figure 24. Applying third step of the workflow on Sentinel-2 image (11 November 2020). The object outline was removed in xii and xiii for better visualization.

5 RESULTS

This chapter follows the goal of the study and presents the OBIA mapped landslide and landslide-dammed classes to show the evolution of the failure and its consequences. The results were presented with maps, 3D models, and 3D web models. In addition, accuracy assessment was applied to compare the results of OBIA with manual mapping.

5.1 OBIA Landslide Mapping

The results of the semi-automatically mapped Kaiwhata landslide and landslide-dammed lake areas were achieved and are presented based on each main landslide activity. The significant changes in the landslide area, the formation of the landslide-dammed lake, and the dam failure, considering the changes in the lake area during the second and third failure were achieved from the analyses. The PlanetScope image is visualized in the result as false-colour image to show the landslide and landslide-dammed lake as visible as possible.

Figure (25 & 26) show the landslide changes during the first main activity. The results from 2017 and 2018 reflect slight changes in the extent of the landslide. The changes show how the landslide was evolving continuously. The landslide was activated in two separate but adjacent areas. Over time, the parts evolved and the vegetation between them disappeared. The result from 16 January 2018 shows that the two separate landslide failures reached each other, however, vegetation between the adjacent parts still existed, and it was concluded to exclude it from the landslide. The vegetated area diminished in the image from 13 September 2018 and the landslide became relatively unmixed. The topographic features of the area and the precipitation formed two water streams from the upper part and caused erosion and incision, resulting in new small slope failures that are visible in the image from 12 November 2018. The erosion continued over time and destabilised the entire slope, likely leading to the second landslide failure.
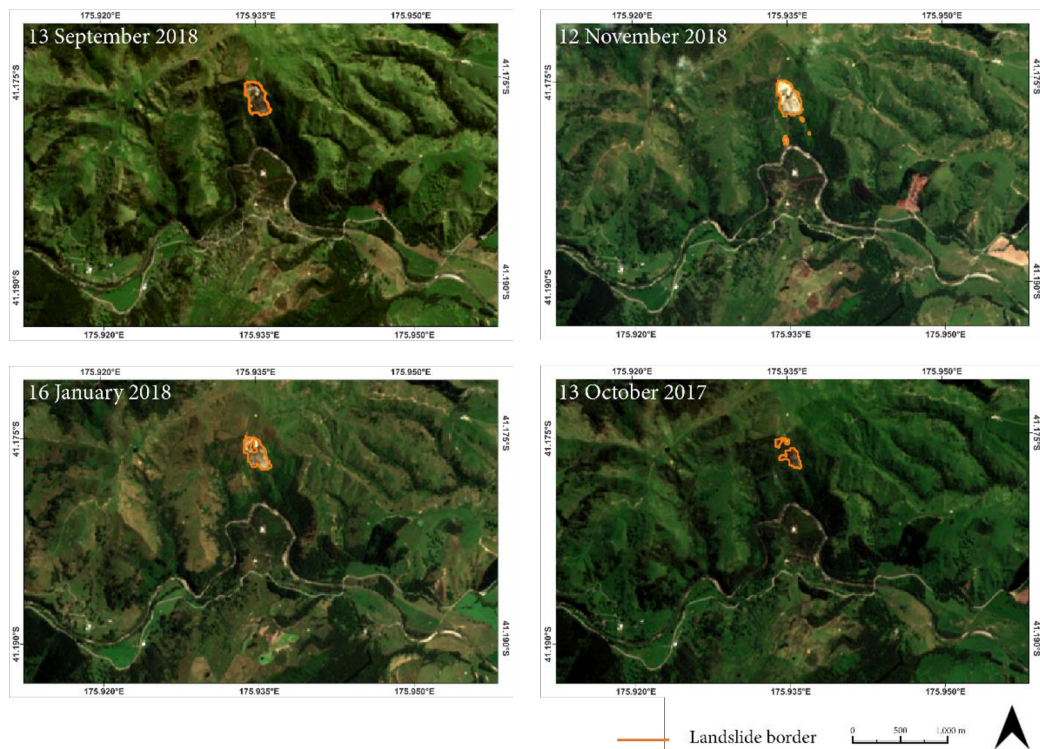

Figure 25. OBIA mapping results for Kaiwhata landslide during first main activity
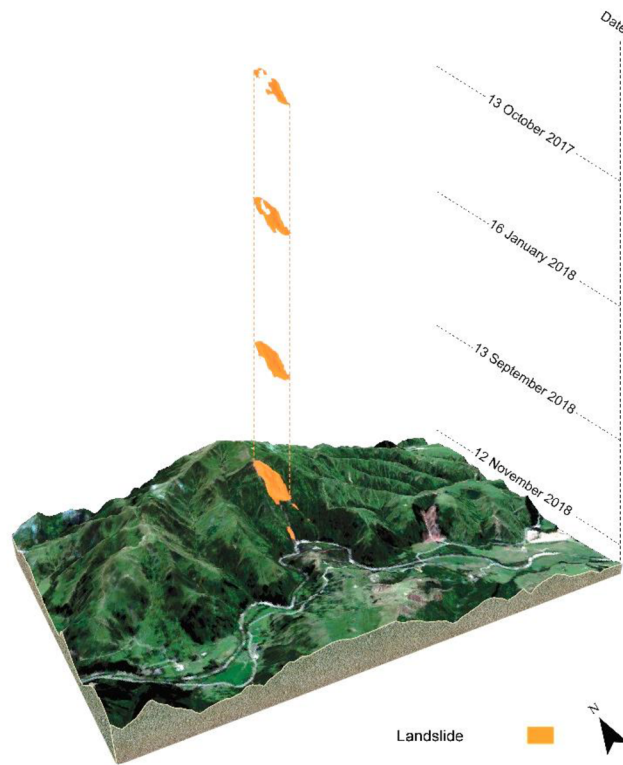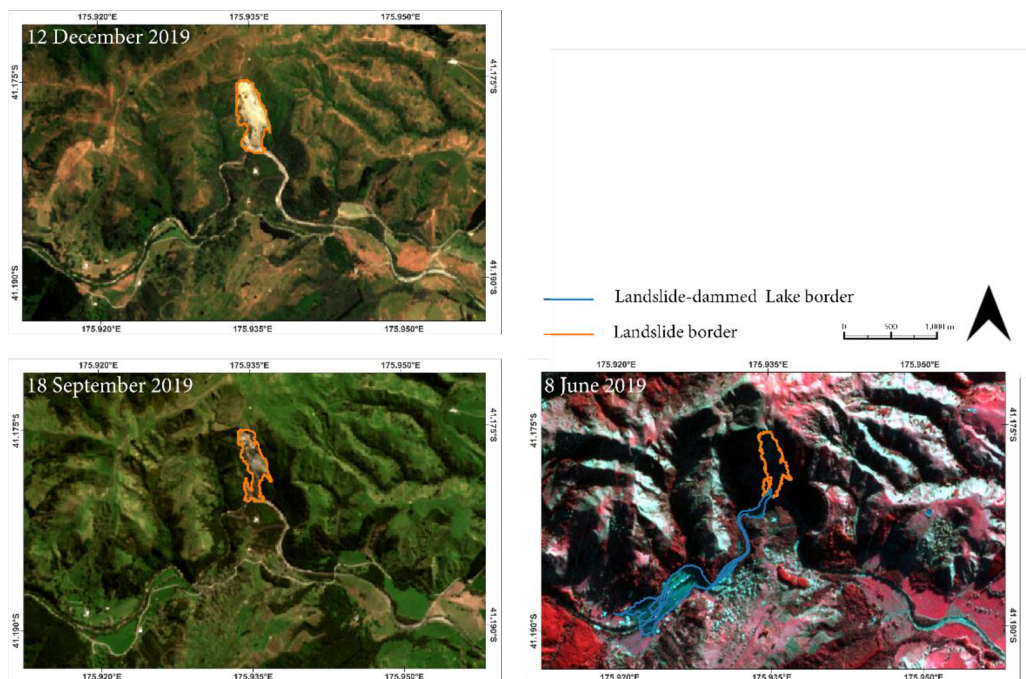
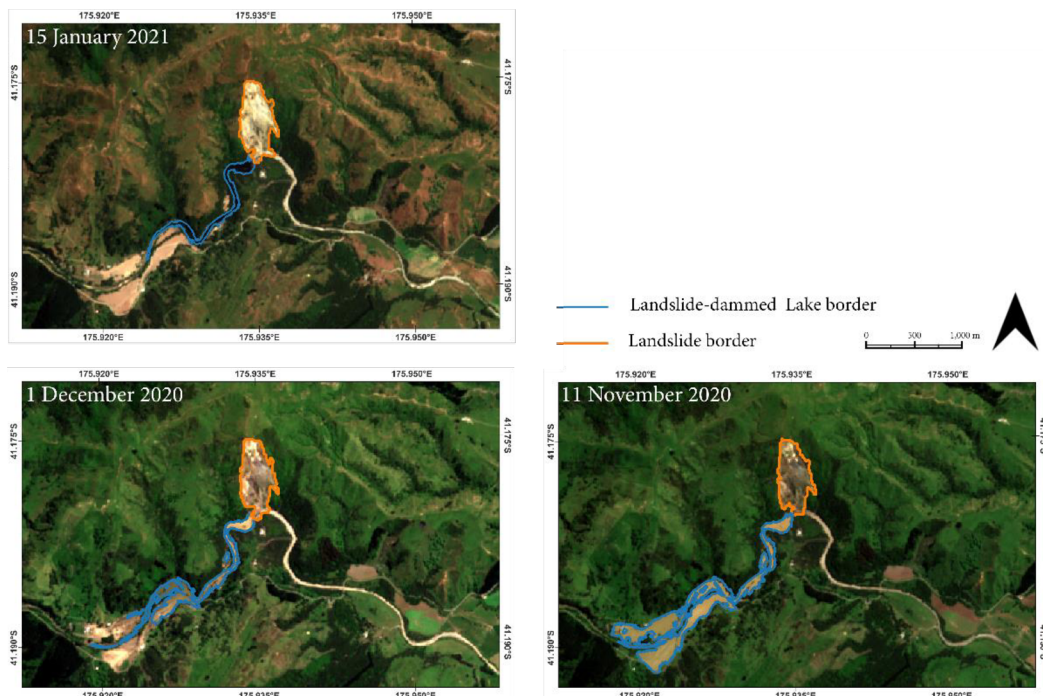**Figure 26. Evolution of landslide during the first main activity**

The second failure of the landslide in summer 2019 was triggered by intense rainfall. The separate slight landslides became a major landslide and formed a landslide-dammed lake since the debris flow reached the Kaiwhata riverbed and blocked the stream, the dam failed after two weeks. The landslide continued to evolve gradually; however, significant changes occurred in November 2020. Figure (27 & 28) show the changes during the second major activity of the Kaiwhata landslide.

Figure 27. OBIA mapping results for Kaiwhata landslide during second main activity

39
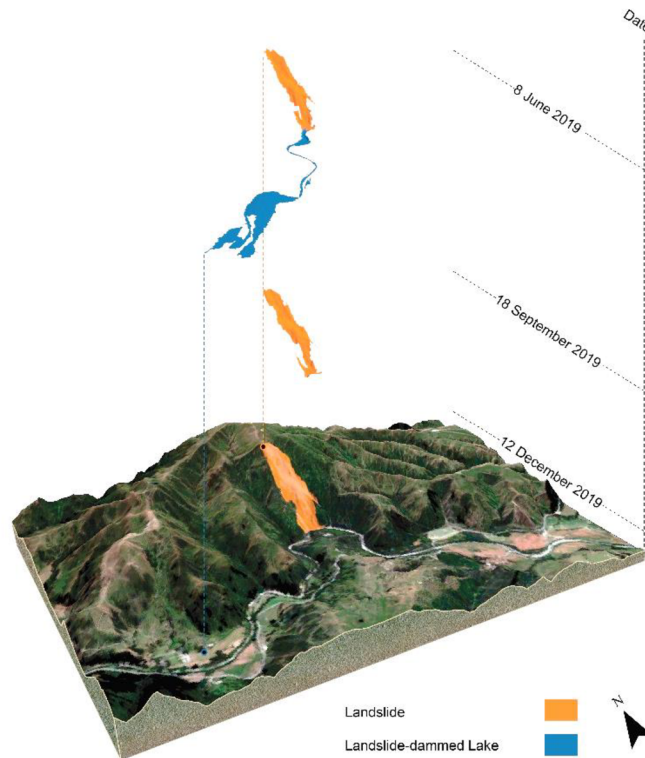
Figure 28. Evolution of landslide during the second main activity

Due to the intense rainfall in November 2020 (GNS Science, 2021), the landslide area was extended, and large amount of debris flow blocked the river. As the result, larger lake formed by the intense rainfall that remained for more than six weeks until the lake overtopped the dam and joined the downstream completely (Figure 29 & 30).

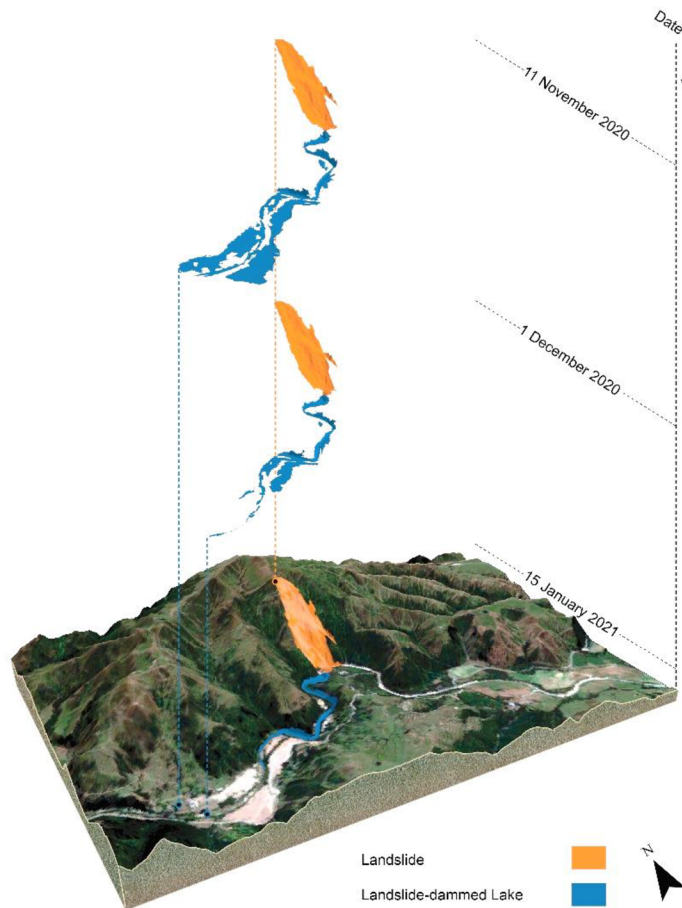**Figure 29. OBIA mapping results for Kaiwhata landslide during third main activity**

Figure 30. Evolution of landslide during the third main activity

Information regarding the evolution of the Kaiwhata landslide and the landslide-dammed lake area on each date is shown in Figure (31). The information shows the moderate increase in the size of the landslide; however, the significant changes were accompanied by the formation of landslide-dammed lake.
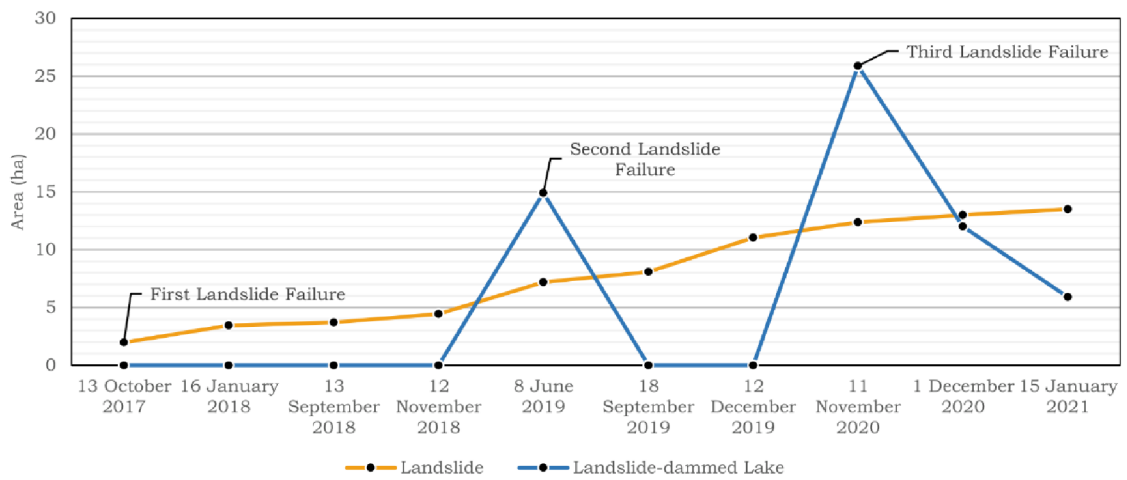

Figure 31. Time series of the Kaiwhata landslide and landslide-dammed lake area evolution

The landslide-dammed lake on 11 November 2020 reached the largest extent with more than 25 acres and affected infrastructure and settlements. Figure (32) shows the flooded lands and farmlands, the flooded Kaiwhata road, and affected buildings and power line infrastructure.
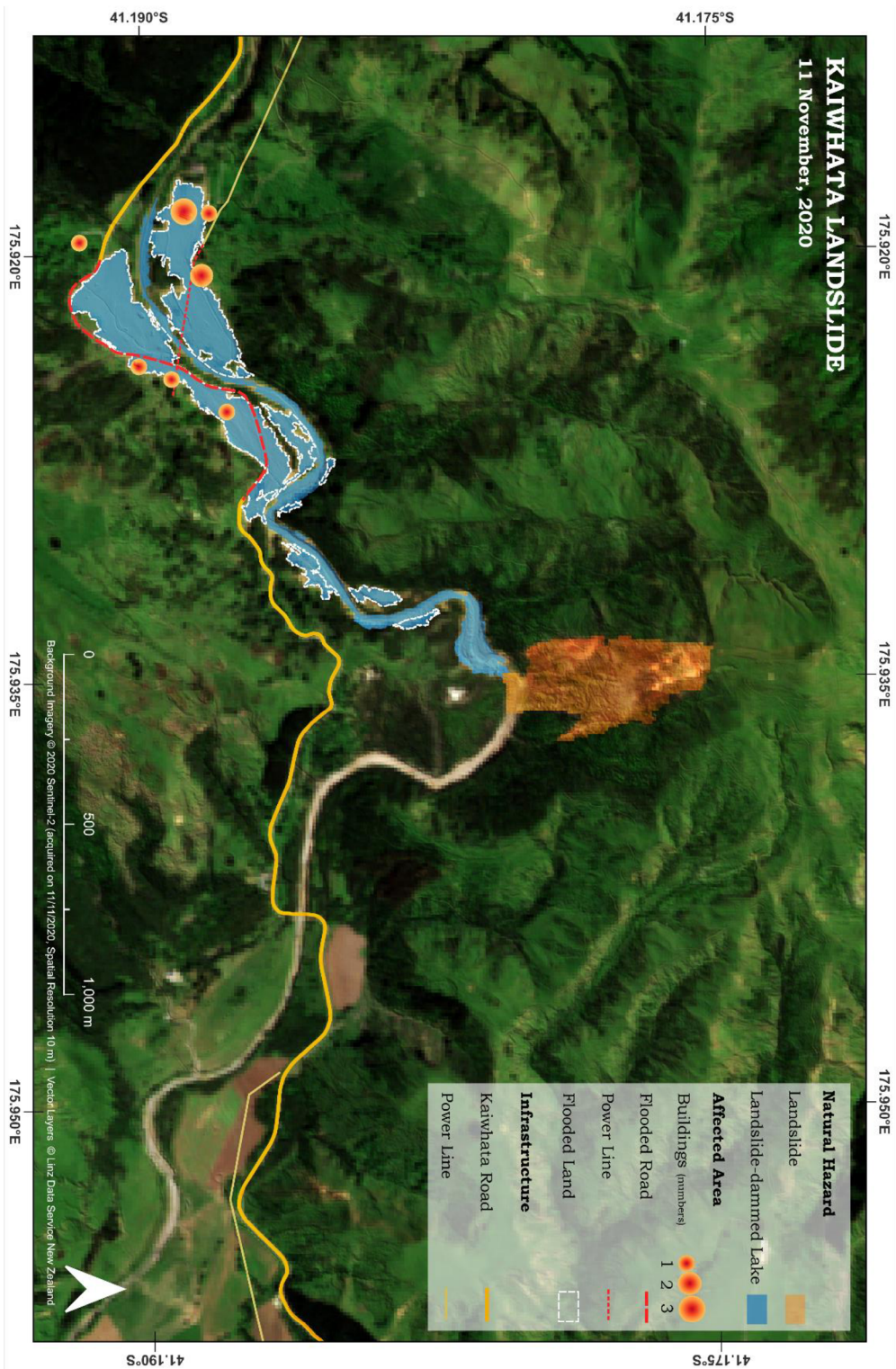

Figure 32. OBIA mapped Landslide and Landslide-dammed Lake together with affected areas (Sentinel-2 11 November 2020)

5.2 Accuracy Assessment

The semi-automated OBIA results were compared with the results from visual interpretation to assess the accuracy of the mapped areas. To do so, manual digitisation at a scale of 1:10,000 was performed for all the images. The producer's accuracy was calculated by dividing the overlap area by the area of the reference data (i.e., the manual mapping result), and the user's accuracy was calculated by dividing the overlap area by the OBIA mapping result. The difference reflects the percentage of the area that was covered in OBIA mapping but not in manual mapping. The negative value of the difference shows that the area mapped manually is larger than the area mapped by OBIA.

Table 6. OBIA and manual mapping (MM) results, the difference between OBIA and MM results, overlapping area and producer's and user's accuracy

Image	Class	OBIA Mapping (ha)	Manual Mapping (ha)	Difference OBIA-MM (%)	Overlap Area (ha)	Producer's Accuracy (%)	User's Accuracy (%)
13 October 2017	Landslide	1.98	2.21	- 10.41	1.84	83.25	92.92
16 January 2018	Landslide	3.46	3.42	1.16	3.10	90.64	89.59
13 September 2018	Landslide	3.72	3.69	0.71	3.37	91.32	90.59
12 November 2018	Landslide	4.45	4.24	4.72	3.94	92.92	88.53
8 June 2019	Landslide	7.20	7.10	1.39	6.50	91.54	90.27
	Landslide-dammed Lake	14.91	19.76	- 24.55	13.45	68.09	90.20
18 September 2019	Landslide	7.97	8.11	- 1.73	7.31	90.13	91.71
12 December 2019	Landslide	11.03	11.03	0	10.51	95.28	95.28
11 November 2020	Landslide	12.29	12.58	- 2.31	12.04	95.7	97.96
	Landslide-dammed Lake	25.88	32.73	- 20.92	24.28	74.18	93.81
1 December 2020	Landslide	13.01	13.30	- 2.19	12.45	93.6	95.69
	Landslide-dammed Lake	12.03	12.79	-5.95	10.43	81.54	86.69
15 January 2021	Landslide	13.32	13.67	- 2.57	12.66	92.61	90.54
	Landslide-dammed Lake	5.76	5.05	12.24	4.55	90.09	78.99

The producer's and user's accuracies for the landslide and landslide-dammed lake areas resulted in different values. The mixture of sparse vegetation with the landslide area and the uncertain intersecting border between landslide and landslide-dammed lake

influenced the final validation results. The highest difference between OBIA and manual mapping for the landslide was related to the image from 13 October 2017. Considering the high user's accuracy value on this date, it confirmed the assumption that manual mapping included larger areas and therefore, the producer's accuracy related to this date was the lowest. The values related to 12 November 2018 showed that the producer mapped a smaller extent than the OBIA-based mapped areas and ignored the small separated slope failures and therefore, the producer's accuracy was much higher than the user's accuracy. The lower producer's accuracy for landslide-dammed lake on 8 June 2019 and 11 November 2020 resulted from the existing dense vegetation along the river. These were the dates when the extent of landslide-dammed lake was the largest and therefore, the mixture of water and the surrounded vegetation was relatively high. The producer's manual delineation considered vegetated areas mixed with the lake as the landslide-dammed lake. Meanwhile, the model excluded them due to high NDVI value and considerable extent of them. However, the comparison between OBIA results and manual mapping should be considered with care since any manual reference data comes with a certain degree of uncertainty.

5.3 3D Web Visualization

QGIS2threejs provided the capability to generate 3D web model for visualizing the results of this study. By transforming 2D mapped results into 3D visualizations, it allowed exploring and interacting with the transformed landslide and landslide dammed classes in a 3D environment. The 3D web visualization was constructed using the DEM data and texturized using the satellite images. The OBIA results were modified to be clickable to provide an attribute table as a pop-up giving information about the mean values of the classification parameters. The generated application can be rotated, zoomed, and panned to view the data from different angles and perspectives. In order to improve the comprehension of the 3D Web visualization, set of narratives combined with motions were added to the model to inform the user about the area of interest, the story behind the cycle of incidents, and the applied OBIA methodology. The visualization was published on Github and is accessible via https://kiapooladsaz.github.io/Kaiwhata.Landslide/. Figure (33) shows the interface of the 3D web visualization application.
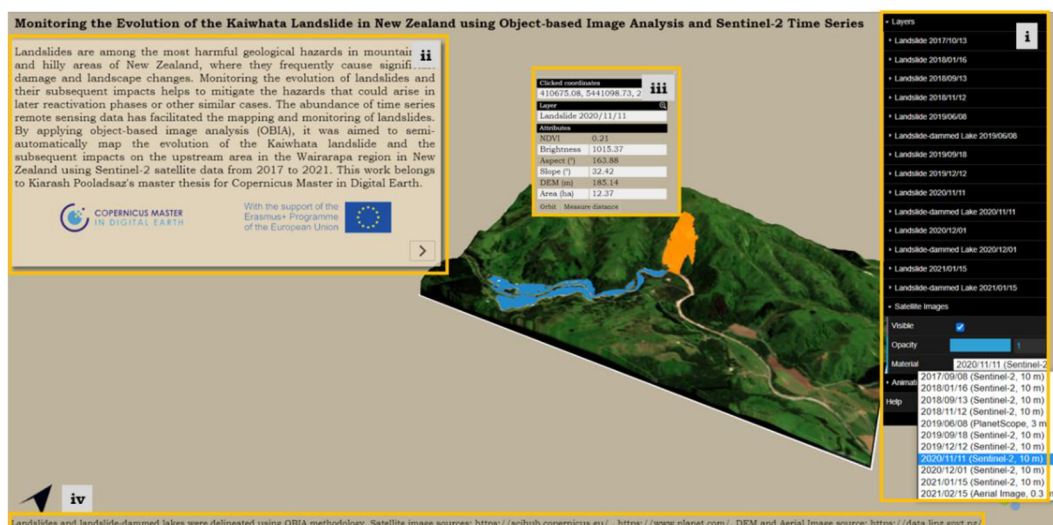

Figure 33. The Interface of 3D Web Visualization; i) OBIA results and satellite images layers, ii) Series of narratives to introduce the AOI and OBIA methodology, iii) Pop-up attribute table, iv) Data resources

44

6 DISCUSSION

Suitability of EO and topographic data to monitor landslide evolution

The utilization of EO data holds immense potential in monitoring the dynamic evolution of landslides. The availability of a rich dataset from Sentinel-2 has proven invaluable in this regard. The spatial resolution of Sentinel-2 images were acceptable enough to monitor a major landslide and the results were satisfactory. However, the presence of cloud coverage has posed limitations to monitor the landslide with higher number of images, as it restricts access to data particularly during the second activity phase. PlanetScope imagery provided suitable data to fill the gap and monitor the Kaiwhata landslide during the second activity phase with higher spatial resolution. Meanwhile, the topographic characteristics of the study area contributed to the formation of a substantial shadow on the landslide during the spring and summer seasons, which affected the quality of PlanetScope imagery, since it was the only image during the mentioned seasons. Therefore, there were challenges when applying the OBIA methodology to map the landslide and landslide-dammed lake. Furthermore, the shadow affected the accuracy assessment procedure when mapping the landslide manually for comparing with the OBIA results. False-colour image composite was used for PlanetScope image to increase the visibility of the desired classes, especially landslide-dammed lake, for visual interpretation and accuracy assessment. In overall, the calculated spectral indices from Sentinel-2 and PlanetScope images that were supported by DEM data helped effectively to monitor the major landslide and the results showed the time series of landslide evolution meaningfully.

The available high spatial resolution DEM data from LINZ data service played a crucial role in the analysis of the Kaiwhata landslide and landslide-dammed lake. The available DEM was created between 2013 and 2014 and was far behind the time span of this study. Nevertheless, thanks to the very high spatial resolution of the DEM, the elevation data and the derivatives helped as the auxiliary layer to distinguish the desired classes from false positive objects and increased the desirability of the results.

Semi-automated multi-scale OBIA methodology

The semi-automated multi-scale OBIA methodology employed an iterative cycle to create a comprehensive knowledge-based workflow. It helped to mitigate the subjectivity in landslide mapping, leading to more reliable and replicable landslide and landslide-dammed lake delineations. The semi-automated nature of the technique, combined with its ability to involve spatial, morphological, and contextual characteristics, made it a valuable tool for mapping and monitoring landslides consistently and reproducibly. This approach also increased the transferability of the workflow to other cases. The development of the analysis approach was formed by a thorough literature review and iterative cycle of trial and error to modify the final workflow that could be applicable to all the images. Furthermore, one noteworthy aspect of this multi-scale segmentation and knowledge-based classification workflow was its ability to adapt to the evolving complexity of the landslide. As the landslide became more intricate over time, the workflow was modified in the way that addressed the changes successfully with minor modifications due to the seasonal changes.

Each step of the analysis was conducted by multiresolution segmentation and set of classification rules. The second step was crucial in mapping the landslide during the second and third landslide activity phase. The landslide reached the riverbed during the mentioned phases and due to the approximate similar spectral characteristics, it was

challenging to distinguish the deposition area of landslide from the riverbed. Applying the segmentation on the unclassified objects from the first step was the turning point of the analysis and helped to map the landslide area effectively. Meanwhile, PlanetScope imagery skipped the second step due to the high spatial resolution of the image. NDVI and NDWI indices were the layers considered for the segmentation to reach objects that were segmented according to the values of the indices. Mapping the landslide-dammed lake was enabled using NDWI index and topographic layers, DEM and slope in multiresolution segmentation for the third step. Topographic feature of the riverbed in addition to the NDWI index provided suitable candidate objects for further classification.

Integration of 3D visualization with landslide mapping methodologies

Qgis2threejs was a powerful user-friendly plugin to create interactive web-based 3D visualization. The plugin allowed converting the 2D landslide and landslide-dammed lake results into a three-dimensional representation. By visualizing the terrain in 3D environment, it clearly helped to understand the topography and identify the patterns to provide valuable insight about the evolution of the landslide that might not be significantly visible in a 2D view. The interactive environment let the user to access and explore the OBIA results and the satellite images in a dynamic manner. It allowed to incorporate multiple layers into the 3D visualization besides the pop-up attribute table that provide information about classification parameters value of the results. In addition, the inserted narratives increased the level of information to comprehend the story behind the Kaiwhata landslide and the methodology applied to map the landslides and landslide-dammed lakes. The interactivity, information-richness, and visually appealing characterisitcs of the 3D web visualization made it potentially an effective tool for communication among decision-makers, stakeholders, and the general public to explore the results. Most of the researches related to landslide analysis and mapping have focused mainly on the methodology more than modifying an innovative visualization that could support the methodology strongly. Effective visualization can enhance the interpretation and understanding of landslide and bridge the gap between scientific findings and practical application, supporting decision-making and public awareness in landslide-prone areas.

7 CONCLUSION

Landslides pose significant risks and challenges worldwide, leading to infrastructure damage, loss of life, landscape changes, and economic losses. New Zealand, with its mountainous terrain, intense rainfall patterns, and tectonic activities, is particularly susceptible to landslides. Traditional methods of landslide mapping and monitoring, such as visual interpretation of aerial imagery combined with field surveying, are time-consuming, resource-intensive, and often unavailable in a timely manner. Meanwhile, advancements in EO data and OBIA methodologies have opened up new possibilities for efficient landslide detection and monitoring.

This diploma thesis focused on assessing the efficiency of OBIA methodology, mainly using Sentinel-2 satellite images, to detect and monitor the major Kaiwhata landslide in New Zealand from 2017 to 2021. The objective was to explore the potential of OBIA and evaluate the suitability of multi-temporal Sentinel-2 images for landslide monitoring. Additionally, the study aimed to provide interactive 3D web visualization and storytelling to enhance the comprehension of landslide changes over time.

The findings of the study demonstrated the effectiveness of EO data, particularly Sentinel-2 imagery, in monitoring landslide evolution. Despite challenges such as cloud coverage and shadow effects during certain seasons, the spatial resolution of Sentinel-2 images was sufficient to capture and monitor the major landslide accurately. The study also highlighted the importance of integrating topographic data, such as DEM data, to enhance the accuracy and reliability of landslide mapping.

The semi-automated multi-scale OBIA methodology employed in this study proved valuable for consistent and reproducible landslide mapping. The iterative cycle of trial and error led to the development of a knowledge-based workflow that could be applied to various images and adapt to the evolving complexity of the landslide over time. Modifying an OBIA workflow consisting of multiresolution segmentation with different scales, classification and refinement parameters, using spectral indices such as NDVI, SAVI, pixel brightness, NDWI, and NIR image band combined with topographic features such as DEM, slope, and aspect led to a unique workflow that monitored the Kaiwhata landslide between 2017 and 2021.

Furthermore, the integration of 3D web visualization through the Qgis2threejs plugin provided an interactive and visually appealing platform to explore and comprehend the landslide results. The 3D visualization facilitated a better understanding of the topography and allowed for the identification of patterns that may not be readily visible in a 2D view. The interactive nature of the visualization, coupled with informative narratives, made it a potentially effective communication tool for decision-makers, stakeholders, and the public in landslide-prone areas.

In conclusion, this study demonstrated the efficiency of OBIA methodology, supported by EO data and topographic information, in monitoring landslide evolution. The results highlighted the benefits of using Sentinel-2 imagery and the multi-scale OBIA approach for accurate landslide mapping. The integration of 3D web visualization enhanced the interpretation and understanding of landslide dynamics, bridging the gap between scientific findings and practical application. The findings of this study can contribute to better landslide management, decision-making, and public awareness in New Zealand and other landslide-prone regions.

LIST OF FIGURES

LIST OF TABLES

REFERENCES

ABAD, L., HÖLBLING, D., SPIEKERMANN, R., PRASICEK, G., DABIRI, Z., & ARGENTIN, A. L. (2022). Detecting landslide-dammed lakes on Sentinel-2 imagery and monitoring their spatio-temporal evolution following the Kaikōura earthquake in New Zealand. Science of the Total Environment, 820, 153335. https://doi.org/10.1016/j.scitotenv.2022.153335

ALEXANDER, D. (2005). Vulnerability to landslides. Landslide hazard and risk, 175-198. https://doi.org/10.1002/9780470012659.ch5

AMATYA, P., KIRSCHBAUM, D., STANLEY, T., & TANYAS, H. (2021). Landslide mapping using object-based image analysis and open source tools. Engineering Geology, 282, 106000. https://doi.org/10.1016/j.enggeo.2021.106000

ANSELM, M. (2020) Properties under Treat after Landslide. Retrieved from https://www.rnz.co.nz/news/ldr/430482/properties-under-threat-after-landslide

BAATZ, M., & SCHAPE, A. (2000) Multiresolution Segmentation: An Optimization Approach for High Quality Multi-Scale Image Segmentation. In: Strobl, J., Blaschke, T. and Griesbner, G., Eds., Angewandte Geographische Informations-Verarbeitung, XII, Wichmann Verlag, Karlsruhe, Germany, 12-23.

BEHLING, R., ROESSNER, S., KAUFMANN, H., & KLEINSCHMIT, B. (2014). Automated spatiotemporal landslide mapping over large areas using rapid-eye time series data. Remote Sensing, 6(9), 8026-8055. https://doi.org/10.3390/rs6098026

BLASCHKE, T. (2010). Object based image analysis for remote sensing. ISPRS journal of photogrammetry and remote sensing, 65(1), 2-16. https://doi.org/10.1016/j.isprsjprs.2009.06.004

BLASCHKE, T., HAY, G. J., KELLY, M., LANG, S., HOFMANN, P., ADDINK, E., ... & TIEDE, D. (2014). Geographic object-based image analysis–towards a new paradigm. ISPRS journal of photogrammetry and remote sensing, 87, 180-191. https://doi.org/10.1016/j.isprsjprs.2013.09.014

BLASCHKE, T., & STROBL, J. (2001). What is wrong with pixels? Some recent developments interfacing remote sensing and GIS. Zeitschrift für Geoinformationssysteme, 12-17.

CRUDEN, D. M. (1991). A simple definition of a landslide. Bulletin of the International Association of Engineering Geology-Bulletin de l'Association Internationale de Géologie de l'Ingénieur, 43(1), 27-29. https://doi.org/10.1007/BF02590167

CRUDEN, D. M.; VARNES, D. J. (1996): Landslide types and processes. In: Turner, A. K.; Schuster, R. L. (Eds.): Landslides: Investigation and Mitigation. Transportation Research Board Special Report 247. National Research Council, pp. 36-75.

DABIRI, Z., HÖLBLING, D., ABAD, L., HELGASON, J. K., SÆMUNDSSON, Þ., & TIEDE, D. (2020). Assessment of landslide-induced geomorphological changes in Hítardalur Valley, Iceland, using Sentinel-1 and Sentinel-2 data. Applied Sciences, 10(17), 5848. https://doi.org/10.3390/app10175848

DAVIES, T. (2015). Landslide hazards, risks, and disasters: introduction. In Landslide Hazards, Risks, and Disasters (pp. 1-16). Academic Press. https://doi.org/10.1016/B978-0-12-396452-6.00001-X

DHONJU, H. K., XIAO, W., MILLS, J. P., & SARHOSIS, V. (2018). Share Our Cultural Heritage (SOCH): worldwide 3D heritage reconstruction and visualization via web and mobile GIS. ISPRS International Journal of Geo-Information, 7(9), 360. https://doi.org/10.3390/ijgi7090360

DRĂGUȚ, L., TIEDE, D., & LEVICK, S. R. (2010). ESP: a tool to estimate scale parameter for multiresolution image segmentation of remotely sensed data. International Journal of Geographical Information Science, 24(6), 859-871. https://doi.org/10.1080/13658810903174803

DRUSCH, M., DEL BELLO, U., CARLIER, S., COLIN, O., FERNANDEZ, V., GASCON, F., ... & BARGELLINI, P. (2012). Sentinel-2: ESA's optical high-resolution mission for GMES operational services. Remote sensing of Environment, 120, 25-36. https://doi.org/10.1016/j.rse.2011.11.026

EVANGELIDIS, K., PAPADOPOULOS, T., PAPATHEODOROU, K., MASTOROKOSTAS, P., & HILAS, C. (2018). 3D geospatial visualizations: Animation and motion effects on spatial objects. Computers & geosciences, 111, 200-212. https://doi.org/10.1016/j.cageo.2017.11.007

FEIZIZADEH, B., BLASCHKE, T., TIEDE, D., & MOGHADDAM, M. H. R. (2017). Evaluating fuzzy operators of an object-based image analysis for detecting landslides and their changes. Geomorphology, 293, 240-254. https://doi.org/10.1016/j.geomorph.2017.06.002

FIORUCCI, F., ARDIZZONE, F., MONDINI, A. C., VIERO, A., & GUZZETTI, F. (2019). Visual interpretation of stereoscopic NDVI satellite images to map rainfall-induced landslides. Landslides, 16, 165-174. https://doi.org/10.1007/s10346-018-1069-y

GNS SCIENCE. (2021). the Kaiwhata Landslide Dam. Retrieved from https://slidenz.net/theme-3/the-kaiwhata-landslide-dam/

GUZZETTI, F., MONDINI, A. C., CARDINALI, M., FIORUCCI, F., SANTANGELO, M., & CHANG, K. T. (2012). Landslide inventory maps: New tools for an old problem. Earth-Science Reviews, 112(1-2), 42-66. https://doi.org/10.1016/j.earscirev.2012.02.001

HAY, G. J., & CASTILLA, G. (2008). Geographic Object-Based Image Analysis (GEOBIA): A new name for a new discipline. Object-based image analysis: Spatial concepts for knowledge-driven remote sensing applications, 75-89. https://doi.org/10.1007/978-3-540-77058-9_4

HELENO, S., MATIAS, M., PINA, P., & SOUSA, A. J. (2016). Semi-automated object-based classification of rain-induced landslides with VHR multispectral images on Madeira Island. Natural Hazards and Earth System Sciences, 16(4), 1035-1048. https://doi.org/10.5194/nhess-16-1035-2016

HÖLBLING, D. (2022). Data and knowledge integration for object-based landslide mapping–challenges, opportunities and applications. gis. Science. Die Zeitschrift für Geoinformatik, 2022(1), 1-13.

HÖLBLING, D., BETTS, H., SPIEKERMANN, R., & PHILLIPS, C. (2016). Identifying spatio-temporal landslide hotspots on North Island, New Zealand, by analysing historical and recent aerial photography. Geosciences, 6(4), 48. https://doi.org/10.3390/geosciences6040048

HÖLBLING, D., EISANK, C., ALBRECHT, F., VECCHIOTTI, F., FRIEDL, B., WEINKE, E., & KOCIU, A. (2017). Comparing manual and semi-automated landslide mapping based on optical satellite images from different sensors. Geosciences, 7(2), 37. https://doi.org/10.3390/geosciences7020037

HÖLBLING, D., FRIEDL, B., & EISANK, C. (2015). An object-based approach for semi-automated landslide change detection and attribution of changes to landslide classes in northern Taiwan. Earth Science Informatics, 8(2), 327-335. https://doi.org/10.1007/s12145-015-0217-3

HÖLBLING, D., FÜREDER, P., ANTOLINI, F., CIGNA, F., CASAGLI, N., & LANG, S. (2012). A semi-automated object-based approach for landslide detection validated by persistent scatterer interferometry measures and landslide inventories. Remote Sensing, 4(5), 1310-1336. https://doi.org/10.3390/rs4051310

HÖLBLING, D., ABAD, L., DABIRI, Z., PRASICEK, G., TSAI, T. T., & ARGENTIN, A. L. (2020). Mapping and analysing the evolution of the Butangbunasi landslide using Landsat time series with respect to heavy rainfall events during Typhoons. Applied Sciences, 10(2), 630. https://doi.org/10.3390/app10020630

HUNGR, O., LEROUEIL, S., & PICARELLI, L. (2014). The Varnes classification of landslide types, an update. Landslides, 11, 167-194. https://doi.org/10.1007/s10346-013-0436-y

HUNTER, J., BROOKING, C., READING, L., & VINK, S. (2016). A Web-based system enabling the integration, analysis, and 3D sub-surface visualization of groundwater monitoring data and geological models. International Journal of Digital Earth, 9(2), 197-214. https://doi.org/10.1080/17538947.2014.1002866

JUŘÍK, V., HERMAN, L., SNOPKOVA, D., GALANG, A. J., STACHOŇ, Z., CHMELÍK, J., ... & ŠAŠINKA, Č. (2020). The 3D hype: Evaluating the potential of real 3D visualization in geo-related applications. Plos one, 15(5), e0233353. https://doi.org/10.1371/journal.pone.0233353

KARANTANELLIS, E., MARINOS, V., VASSILAKIS, E., & CHRISTARAS, B. (2020). Object-based analysis using unmanned aerial vehicles (UAVs) for site-specific landslide assessment. Remote Sensing, 12(11), 1711. https://doi.org/10.3390/rs12111711

LAHOUSSE, T., CHANG, K. T., & LIN, Y. H. (2011). Landslide mapping with multi-scale object-based image analysis–a case study in the Baichi watershed, Taiwan. Natural Hazards and Earth System Sciences, 11(10), 2715-2726. https://doi.org/10.5194/nhess-11-2715-2011

LANG, S., & BLASCHKE, T. (2006). Bridging remote sensing and GIS – what are the main supporting pillars? International Archives of Photogrammetry, Remote Sensing and Spatial Information Sciences, 1-5.

LANG, S., & TIEDE, D. (2018). Geospatial data integration in OBIA: implications of accuracy and validity. In Remote Sensing Handbook-Three Volume Set (pp. 329-350). CRC Press. https://doi.org/10.1201/b19294

LISSAK, C., BARTSCH, A., DE MICHELE, M., GOMEZ, C., MAQUAIRE, O., RAUCOULES, D., & ROULLAND, T. (2020). Remote sensing for assessing landslides and associated hazards. Surveys in Geophysics, 41, 1391-1435. https://doi.org/10.1007/s10712-020-09609-1

LITHOFILE (2020, November 27). Reactivated Landslide Dam. Kaiwhata River, New Zealand. [Online forum]. Retrieved from https://www.reddit.com/r/geomorphology/comments/k1xp51/reactivated_landslide_dam_kaiwhata_river_new/

LU, P., QIN, Y., LI, Z., MONDINI, A. C., & CASAGLI, N. (2019). Landslide mapping from multi-sensor data through improved change detection-based Markov random field. Remote Sensing of Environment, 231, 111235. https://doi.org/10.1016/j.rse.2019.111235

MARTHA, T. R., KAMALA, P., JOSE, J., VINOD KUMAR, K., & JAI SANKAR, G. (2016). Identification of new landslides from high-resolution satellite data covering a large area using object-based change detection methods. Journal of the Indian Society of Remote Sensing, 44(4), 515-524. https://doi.org/10.1007/s12524-015-0532-7

MARTHA, T.R., KERLE, N., JETTEN, V.G., WESTEN, C.J., & KUMAR, K.V. (2010). Characterising spectral, spatial and morphometric properties of landslides for semi-automatic detection using object-oriented methods. Geomorphology, 116, 24-36. https://doi.org/10.1016/j.geomorph.2009.10.004

MONDINI, A. C., GUZZETTI, F., CHANG, K. T., MONSERRAT, O., MARTHA, T. R., & MANCONI, A. (2021). Landslide failures detection and mapping using Synthetic Aperture Radar: Past, present and future. Earth-Science Reviews, 216, 103574. https://doi.org/10.1016/j.earscirev.2021.103574

MORA, O. E., LENZANO, M. G., TOTH, C. K., GREJNER-BRZEZINSKA, D. A., & FAYNE, J. V. (2018). Landslide change detection based on multi-temporal Airborne LiDAR-derived DEMs. Geosciences, 8(1), 23. https://doi.org/10.3390/geosciences8010023

MORGENSTERN, R., MASSEY, C., ROSSER, B., & ARCHIBALD, G. (2021). Landslide dam hazards: assessing their formation, failure modes, longevity and downstream impacts. Understanding and Reducing Landslide Disaster Risk: Volume 5 Catastrophic Landslides and Frontiers of Landslide Science 5th, 117-123. https://doi.org/10.1007/978-3-030-60319-9_12

PAWŁUSZEK, K., MARCZAK, S., BORKOWSKI, A., & TAROLLI, P. (2019). Multi-aspect analysis of object-oriented landslide detection based on an extended set of LiDAR-derived terrain features. ISPRS International Journal of Geo-Information, 8(8), 321. https://doi.org/10.3390/ijgi8080321

PETLEY, D. (2012). Global patterns of loss of life from landslides. Geology 2012; 40 (10): 927–930. https://doi.org/10.1130/G33217.1

PETLEY, D. The landslide blog. Examples of landslides in New Zealand, [online forum]. Retrieved from https://blogs.agu.org/landslideblog/

PLANK, S., TWELE, A., & MARTINIS, S. (2016). Landslide mapping in vegetated areas using change detection based on optical and polarimetric SAR data. Remote Sensing, 8(4), 307. https://doi.org/10.3390/rs8040307

PREPPERNAU, C. A., & JENNY, B. (2015). Three-dimensional versus conventional volcanic hazard maps. Natural Hazards, 78, 1329-1347. https://doi.org/10.1007/s11069-015-1773-z

ROSSER, B. (2019) Landslide Dam at Kaiwhata River. Retrieved from https://www.geonet.org.nz/news/3SF3C5Qz6k8MSGXmVUPDcn

ROSSER, B. (2019) Update on Landslide Dam at Kaiwhata River. Retrieved from https://www.geonet.org.nz/news/2qwgEidlRAVZWs5J0iUBvu

ROSSER, B., DELLOW, S., HAUBROCK, S., & GLASSEY, P. (2017). New Zealand's national landslide database. Landslides, 14(6), 1949-1959. https://doi.org/10.1007/s10346-017-0843-6

SIEBER, R., EICHENBERGER, R., & HURNI, L. (2019). 3D Carto-Graphics-Principles, Methods and Examples for Interactive Atlases. Abstracts of the ICA, 1, NA-NA. https://doi.org/10.5194/ica-abs-1-338-2019

STUMPF, A., & KERLE, N. (2011). Object-oriented mapping of landslides using Random Forests. Remote sensing of environment, 115(10), 2564-2577. https://doi.org/10.1016/j.rse.2011.05.013

THÖNY, M., SCHNÜRER, R., SIEBER, R., HURNI, L., & PAJAROLA, R. (2018). Storytelling in interactive 3D geographic visualization systems. ISPRS International Journal of Geo-Information, 7(3), 123. https://doi.org/10.3390/ijgi7030123

TIEDE, D., LANG, S., ALBRECHT, F., & HÖLBLING, D. (2010). Object-based class modelling for cadastre-constrained delineation of geo-objects. Photogrammetric Engineering & Remote Sensing, 76(2), 193-202. https://doi.org/10.14358/PERS.76.2.193

TOFANI, V., RASPINI, F., CATANI, F., & CASAGLI, N. (2013). Persistent Scatterer Interferometry (PSI) technique for landslide characterization and monitoring. Remote Sensing, 5(3), 1045-1065. https://doi.org/10.3390/rs5031045

TRAVELLETTI, J., DELACOURT, C., ALLEMAND, P., MALET, J. P., SCHMITTBUHL, J., TOUSSAINT, R., & BASTARD, M. (2012). Correlation of multi-temporal ground-based optical images for landslide monitoring: Application, potential and limitations. ISPRS Journal of Photogrammetry and Remote Sensing, 70, 39-55. https://doi.org/10.1016/j.isprsjprs.2012.03.007

UHLEMANN, S., SMITH, A., CHAMBERS, J., DIXON, N., DIJKSTRA, T., HASLAM, E., ... & MACKAY, J. (2016). Assessment of ground-based monitoring techniques applied to landslide investigations. Geomorphology, 253, 438-451. https://doi.org/10.1016/j.geomorph.2015.10.027

VITALIS, S., ARROYO OHORI, K., & STOTER, J. (2020). CityJSON in QGIS: Development of an open-source plugin. Transactions in GIS, 24(5), 1147-1164. https://doi.org/10.1111/tgis.12657

XUN, Z., ZHAO, C., KANG, Y., LIU, X., LIU, Y., & DU, C. (2022). Automatic Extraction of Potential Landslides by Integrating an Optical Remote Sensing Image with an InSAR-Derived Deformation Map. Remote Sensing, 14(11), 2669. https://doi.org/10.3390/rs14112669

YANG, W., WANG, Y., SUN, S., WANG, Y., & MA, C. (2019). Using Sentinel-2 time series to detect slope movement before the Jinsha River landslide. Landslides, 16, 1313-1324. https://doi.org/10.1007/s10346-019-01178-8

ZHONG, C., LIU, Y., GAO, P., CHEN, W., LI, H., HOU, Y., ... & MA, H. (2020). Landslide mapping with remote sensing: challenges and opportunities. International Journal of Remote Sensing, 41(4), 1555-1581. https://doi.org/10.1080/01431161.2019.1672904

WARD, M. O., GRINSTEIN, G., & KEIM, D. (2010). Interactive data visualization: foundations, techniques, and applications. CRC press. ISBN 978-1-4398-6554-5.

LIST OF ATTACHMENTS

Free attachments

Attachment 1   Poster

Attachment 2   Website